# Elevated DNA Damage without signs of aging in the short-sleeping Mexican Cavefish

Evan Lloyd*[1], Fanning Xia*[2], Kinsley Moore[1], Carolina Zertuche[1], Aakriti Rastogi[1], Rob Kozol[3], Olga Kenzior[2], Wesley Warren[4], Lior Appelbaum[5], Rachel L. Moran[1], Chongbei Zhao[2], Erik Duboue[3], Nicolas Rohner[2], and Alex C. Keene[1]

1. Department of Biology, Texas A&M University, College Station, TX 77840
2. Stowers Institute for Medical Research, Kansas City, MO 64110
3. Harriet Wilkes Honors College, Florida Atlantic University, Jupiter, FL 33458
4. Department of Genomics, University of Missouri, Columbia, MO 65211
5. Faculty of Life Science and the Multidisciplinary Brain Research Center, Bar Illan University, Ramat Gan, Israel

* Denotes equal contributions
Address correspondence to nro@stowers.org and keenea@tamu.edu

## Abstract

Dysregulation of sleep has widespread health consequences and represents an enormous health burden. Short-sleeping individuals are predisposed to the effects of neurodegeneration, suggesting a critical role for sleep in the maintenance of neuronal health. While the effects of sleep on cellular function are not completely understood, growing evidence has identified an association between sleep loss and DNA damage, raising the possibility that sleep facilitates efficient DNA repair. The Mexican tetra fish, *Astyanax mexicanus* provides a model to investigate the evolutionary basis for changes in sleep and the consequences of sleep loss. Multiple cave-adapted populations of these fish have evolved to sleep for substantially less time compared to surface populations of the same species without identifiable impacts on healthspan or longevity. To investigate whether the evolved sleep loss is associated with DNA damage and cellular stress, we compared the DNA Damage Response (DDR) and oxidative stress levels between *A. mexicanus* populations. We measured markers of chronic sleep loss and discovered elevated levels of the DNA damage marker γH2AX in the brain, and increased oxidative stress in the gut of cavefish, consistent with chronic sleep deprivation. Notably, we found that acute UV-induced DNA damage elicited an increase in sleep in surface fish but not in cavefish. On a transcriptional level, only the surface fish activated the photoreactivation repair pathway following UV damage. These findings suggest a reduction of the DDR in cavefish compared to surface fish that coincides with elevated DNA damage in cavefish. To examine DDR pathways at a cellular level, we created an embryonic fibroblast cell line from the two populations of *A. mexicanus*. We observed that both the DDR and DNA repair were diminished in the cavefish cells, corroborating the *in vivo* findings and suggesting that the acute response to DNA damage is lost in cavefish. To investigate the

long-term impact of these changes, we compared the transcriptome in the brain and gut of aged surface fish and cavefish. Strikingly, many genes that are differentially expressed between young and old surface fish do not transcriptionally vary by age in cavefish. Taken together, these findings suggest that have developed resilience to sleep loss, despite possessing cellular hallmarks of chronic sleep deprivation.

## Introduction

Sleep is ubiquitous throughout the animal kingdom and has been identified in animals with relatively simple neural networks, including jellyfish and nematodes through primates, suggesting ancient function and shared evolutionary origins [1–5]. While the primary functions of sleep are not fully understood, it is essential for many processes including neural connectivity, clearance of toxic metabolites, immunity, learning, and memory [6–8]. There is growing evidence that DNA damage may play an important role in sleep drive[9–12]. DNA damage is associated with periods of prolonged wakefulness and is reduced during sleep across numerous species, including C. *elegans*, zebrafish, mice, and humans[13–15]. In turn, sleep disruption is associated with DNA damage, and sleep deprivation (SD) inhibits the expression of DNA repair genes in humans [12,14] suggesting a critical role for sleep in the maintenance of genome integrity and function and an association between sleep loss and DNA damage, which could lead to neurodegeneration. Further, chronic sleep loss results in elevated reactive oxygen species (ROS) in the gut and/or brain that contribute to mortality in *Drosophila* and mice [11,16]. Despite these advances, little is known about the cellular consequences of sleep loss the evolutionary relationship between DNA damage and sleep regulation.

Comparative approaches examining evolutionarily derived differences in sleep have provided significant insight into the genetic and functional basis of sleep regulation [4,17,18]. While the majority of sleep studies in fish have used zebrafish, the Mexican tetra *Astyanax mexicanus* is an emerging model for investigating the genetic and evolutionary basis underlying behavioral and physiological traits [19–23]. *A. mexicanus* exists as blind cave populations and an extant surface population that are interfertile. In this system, there are similar sleep loss phenotypes among geographically and geologically isolated cave populations [24,25] with likely unique genetic bases between caves [26–28]. Further, the evolved differences in DNA repair genes, including links between mechanisms regulating sleep, light responsiveness, and DNA repair across all three cave populations studied to date [27,29] These findings support the notion that the genetic and molecular underpinnings of sleep are closely related to DNA repair processes in cavefish.

Examining the ecological factors that contribute to evolved changes in sleep regulation and the physiological consequences of this sleep loss has the potential to address the fundamental functions of sleep. For example, in humans, insomnia is associated with many different diseases and increased morbidity, suggesting that sleep is critical for healthy aging[30,31]. Despite the dramatic reduction in sleep, there are no apparently health consequences to cavefish, suggesting an established resilience to sleep loss[32–34]. Considering that changes in the levels of DNA breaks are associated with sleep regulation in flies, zebrafish, mice, and humans [10,12,35], it is possible that intrinsic changes in the DNA repair and DDR pathways underlie reduced sleep need in cavefish.

Here, we sought to investigate the relationship between DNA damage and the evolution of sleep, to test at the cellular and organismal levels whether cavefish have markers of chronic sleep deprivation and accelerated aging. We find that DNA damage is elevated in cavefish brains, consistent with the notion that sleep loss is associated with elevated levels of DNA damage. The transcriptional and behavioral response to UV damage is blunted in cavefish, and cavefish cells exhibit diminished DNA repair capabilities raising the possibility that reduced DDR function may contribute to sleep loss in cavefish. To examine the long-term consequences of reduced DDR, we examined transcriptional differences in young and aged surface and cavefish. While aging in surface fish is associated with broad transcriptional changes across tissue types, there are relatively few transcriptional differences between young and aged cavefish. Together, these findings reveal that cavefish appear to have developed molecular resilience to aging despite elevated DNA damage that likely derives from sleep loss.

**Results**

In vertebrates, including teleost fish such as zebrafish and *A. mexicanus*, DNA damage activates a highly conserved and stereotypical response and repair program. Markers of DDR proteins can be localized and quantified at the cellular and whole organism levels. Phosphorylation of histone H2AX on serine 139 (γH2AX) offers a well-established and quantifiable biomarker of cellular response to DNA double-strand breaks that is necessary for the assembly of repair complexes [36]. We compared γH2AX between surface fish and Pachón cavefish

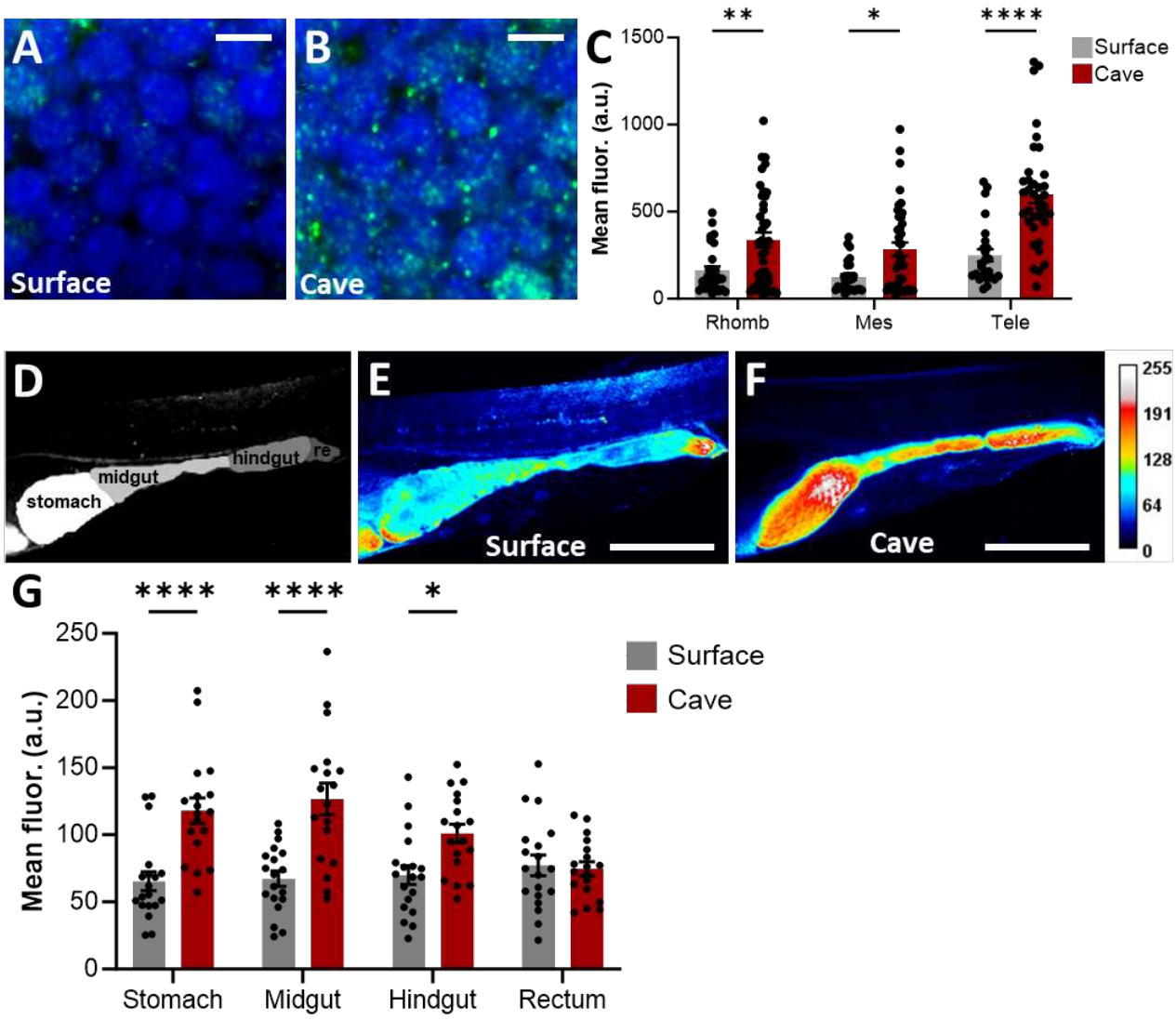


**Figure 1. Cavefish harbor increased neuronal DNA damage and gut ROS. (A,B)** Representative images of cells stained with DAPI and γH2AX in the rhombencephalon of surface fish **(A)** and cavefish **(B)**. Scale bar = 5 μm. **(C)** Mean γH2AX fluorescence across three regions of surface fish and cavefish brains. (rhomb: rhombencephalon; mes: mesencephalon; tele: telencephalon) (Mixed-effects analysis: $F_{1,\ 68} = 32.08$, $p < 0.0001$). **(D)** Representative image of larval gut showing regions in false color (re: rectum). **(E,F)** Representative images of surface fish and cavefish guts stained with DHE marking ROS. Scale bar = 500 μm. **(G)** Mean DHE fluorescence across four regions of surface fish and cavefish guts (two-way repeated measures ANOVA: $F_{1,\ 35} = 48.36$, $p < 0.0001$).

brains at ZT0, a time when both populations are behaviorally activity and sleep is minimal (Fig 1A–B and Supplemental Movie 1). Levels of γH2AX were elevated in the rhombencephalon, telencephalon, and mesencephalon of cavefish compared to surface fish (Fig 1C). These findings suggest that DNA damage is elevated in short-sleeping cavefish compared to their surface fish counterparts.

Sleep loss is associated with reduced gut function, including the accumulation of reactive oxygen species (ROS) [11]. To examine whether markers of sleep loss extend to the gut in *A. mexicanus*, we compared ROS in the guts of surface and cavefish. Fish aged 6 days post fertilization (dpf) were incubated in the ROS marker dihydroethidium (DHE), and guts were imaged on a confocal microscope. We found that ROS in the gut is upregulated in cavefish, reinforcing the idea that cellular stress and canonical markers of DDR are elevated in these short-sleeping fish (Fig 1D–G); ROS levels were elevated in the stomach, midgut, and hindgut, but not in the rectum (Fig 1G). Together, these findings fortify the notion that cellular stress is elevated in the gut of cavefish relative to surface fish.

To further examine the direct link between DNA damage and sleep in *A. mexicanus*, surface fish and cavefish were exposed to short periods of UV-B radiation, known to cause DNA damage and inducing double-stranded breaks [10]. In surface fish, UV exposure resulted in a dose-dependent increase in sleep for up to three hours, similar to findings in zebrafish [10] (Fig 2A and 2B). Interestingly, sleep decreased in surface fish sleep during the nighttime, perhaps the result of sleep credit that derives from increased sleep during the day (Fig 2A) [37] . Increases in sleep amount in surface fish were mediated by both increased bout number, and, at the higher dose, an increase in bout length (Fig 2C and 2D). Conversely, there was no effect of UV treatment on daytime or nighttime sleep in cavefish (Fig 2E–H). Analysis of sleep- and wake-probability was consistent with these measurements, showing elevated sleep pressure and reduced wake pressure in surface fish during the three hours following treatment, whereas in cavefish, there was no change (Fig S1). These results confirm that UV-induced DNA damage promotes sleep in *A. mexicanus* surface fish, whereas this response is lost in cavefish.

To differentiate between these two possibilities, we examined the effects of the high dose (60 seconds) of UV treatment at zeitgeber time (ZT) 0 (onset of lights on) on the transcriptional response in surface fish and cavefish. Fish aged 6 dpf were harvested for RNA extraction 90 minutes following UV exposure (Fig 3A, Supplemental Data 1). PCA analysis of RNA expression showed that the largest factor driving variability across samples was population, with principal component 1 separating samples by

## Surface

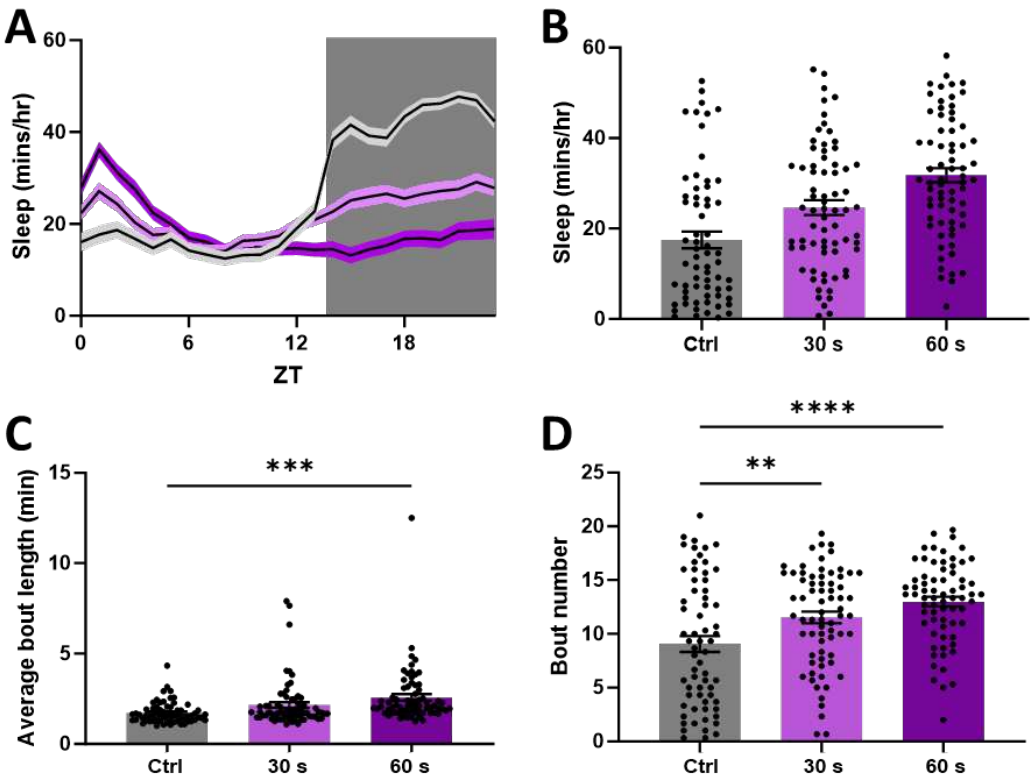


## Cave

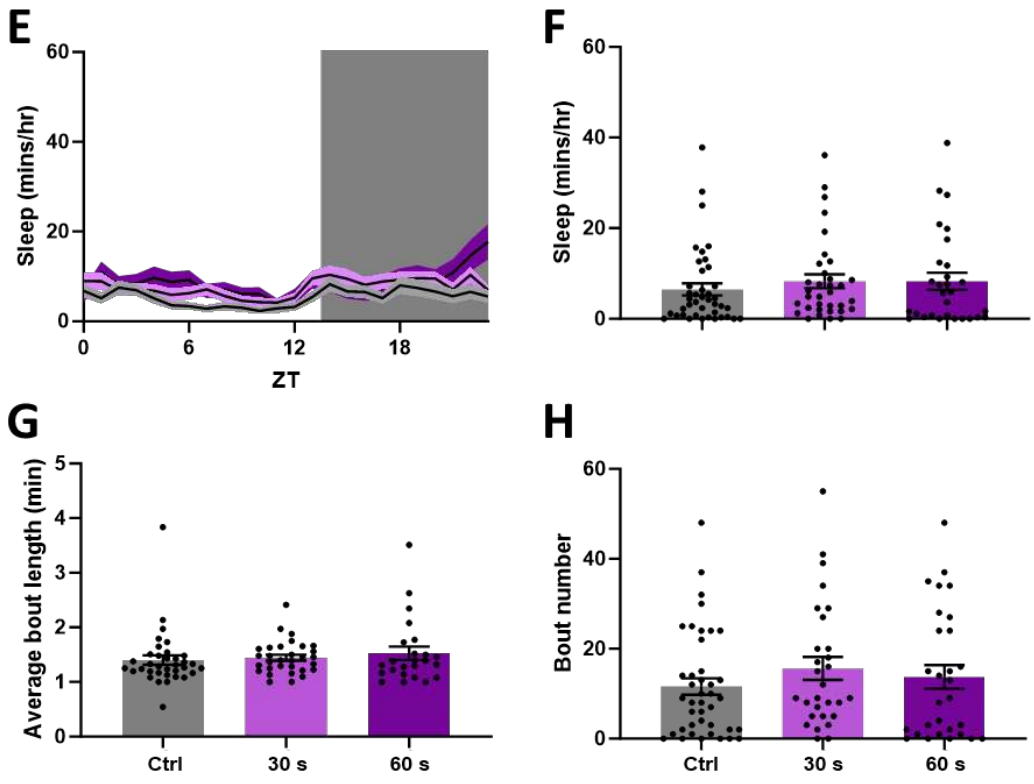

**Figure 2. Cavefish lack a sleep response to UV-B-induced DNA damage. (A)** The 24-hour sleep profiles of surface fish exposed to 30 or 60 seconds of UV-B light compared to controls. **(B)** Average sleep amount in surface fish in the 3 hours following UV-B exposure (one-way ANOVA: $F_{2, 202} = 18.75$, $p < 0.0001$). **(C)** Average bout length in surface fish in the 3 hours following UV-B exposure (one-way ANOVA: $F_{2, 201} = 8.301$, $p = 0.0003$). **(D)** Bout number in the 3 hours following UV-B exposure (one-way ANOVA: $F_{2, 201} = 11.5$, $p < 0.0001$). **(E)** The 24-hour sleep profiles of cavefish exposed to 30 or 60 seconds of UV-B light compared to controls. **(F)** Average sleep amount in cavefish in the 3 hours following UV-B exposure. **(G)** Average bout length in cavefish in the 3 hours following UV-B exposure. **(H)** Bout number in cavefish in the 3 hours following UV-B exposure. (ZT=Zeitgeber time). All treatments performed at ZT0.

population and accounting for 86% of the variance. Principal component 2 separated samples by treatment and accounted for 9% of the variance (Fig 3B). Analysis revealed numerous genes that were differentially expressed in both populations, including upregulation of the RNA Polymerase regulating transcription factor *fosl1a* and downregulation of *spi*-c (Fig 3C). Numerous genes were selectively differentially expressed, including upregulation of the heat shock protein *hspb9* in surface fish and downregulation of the glucose sensor *gck* in cavefish (Fig 3C and Fig S2A,B). To determine if the DDR pathway is activated in cavefish following exposure to UV light, we quantified changes in pathway components in surface fish and cavefish. A heat map of DNA repair genes significantly upregulated in surface fish revealed that several components of DNA repair pathways are differentially expressed in cavefish following UV treatment (Fig 3D). Notably, cyclobutane pyrimidine dimer photolyase (*cpdp)*, an important component of the photoreactivation repair pathway for UV-induced DNA damage, responds strongly in surface fish, but fails to respond in cavefish. Although previous groups have reported that *cpdp* is constitutively upregulated in adult cavefish[29], our analysis did not align with this finding; however, this could be due to differences in the age or circadian timepoint studied. A more detailed analysis of previous circadian transcriptomic studies in cavefish revealed that two of the DDR genes are elevated at some, but not all phases of the circadian cycle (Fig S3). Additionally, *xrcc3*, a paralog of human *rad51* that is important for homologous recombination, and *fan1*, a component of the Fanconi Anemia pathway, are nonresponsive to UV-B treatment in cavefish. Conversely, *ube2al*, which is required for post-replication DNA repair, is perhaps even more strongly activated in cavefish compared to surface fish. Together, these findings suggest that DNA repair processes in cavefish have undergone complex changes, with some pathways rendered nonfunctional, while others may have been upregulated in order to compensate for loss of function in other areas. To understand transcriptional changes more fully as a result of UV-B treatment, gene set enrichment analysis (GSEA) was performed on both surface fish and cavefish. A large number of pathways were enriched in both populations (Fig S2C and S2D); to examine differences between the

transcriptional responses of the two populations, we identified pathways which were specifically enriched in either surface fish or cavefish (Fig 3E). Only surface fish showed significant activation of genes associated with response to ROS and cell redox homeostasis, consistent with measurements of elevated ROS in cavefish, whereas cavefish showed activation of genes associated with metabolic processes and suppression of genes associated with synaptic signaling, suggesting altered responses to DNA damage.

To quantify DNA damage on a cellular level, we established embryonic fibroblast cell lines derived from surface fish and Pachón cavefish embryos (Fig S4A). In brief, we dissociated and sterilized cells from embryos less than 12 hours post fertilization and isolated individual clones that were propagated for over 40 passages. To confirm that the cell lines indeed represented fibroblasts, we stained the cells for the presence of vimentin, a known fibroblast marker [38]. Both cell lines exhibited stable vimentin expression (Fig S4B). We further validated the fibroblast nature of the cell lines by RNA sequencing, which showed enhanced expression of other fibroblast signature genes such as *col1a1* compared to other cell types, including the previously established liver-derived cell lines [39] from the same species, mouse stem cells, and mouse embryonic fibroblasts [40] (Fig S4C).

We next used the newly generated fibroblast cell lines to measure DNA damage level upon UV radiation exposure. We exposed the cells to 100 J/m$^2$ UV radiation and visualized UV-induced DNA lesions using an antibody targeting cyclobutene pyrimidine dimer (CPD) as a DNA damage marker. Both the surface fish and cavefish-derived cell lines exhibited strong CPD induction, indicating pronounced UV-induced DNA damage (Fig 4A). We quantified the mean fluorescence per nucleus area using the Cellpose function [41] of ImageJ and found no significant difference between the two derived cell lines ($p$ = 0.6404, two-way ANOVA, Fig 4B).

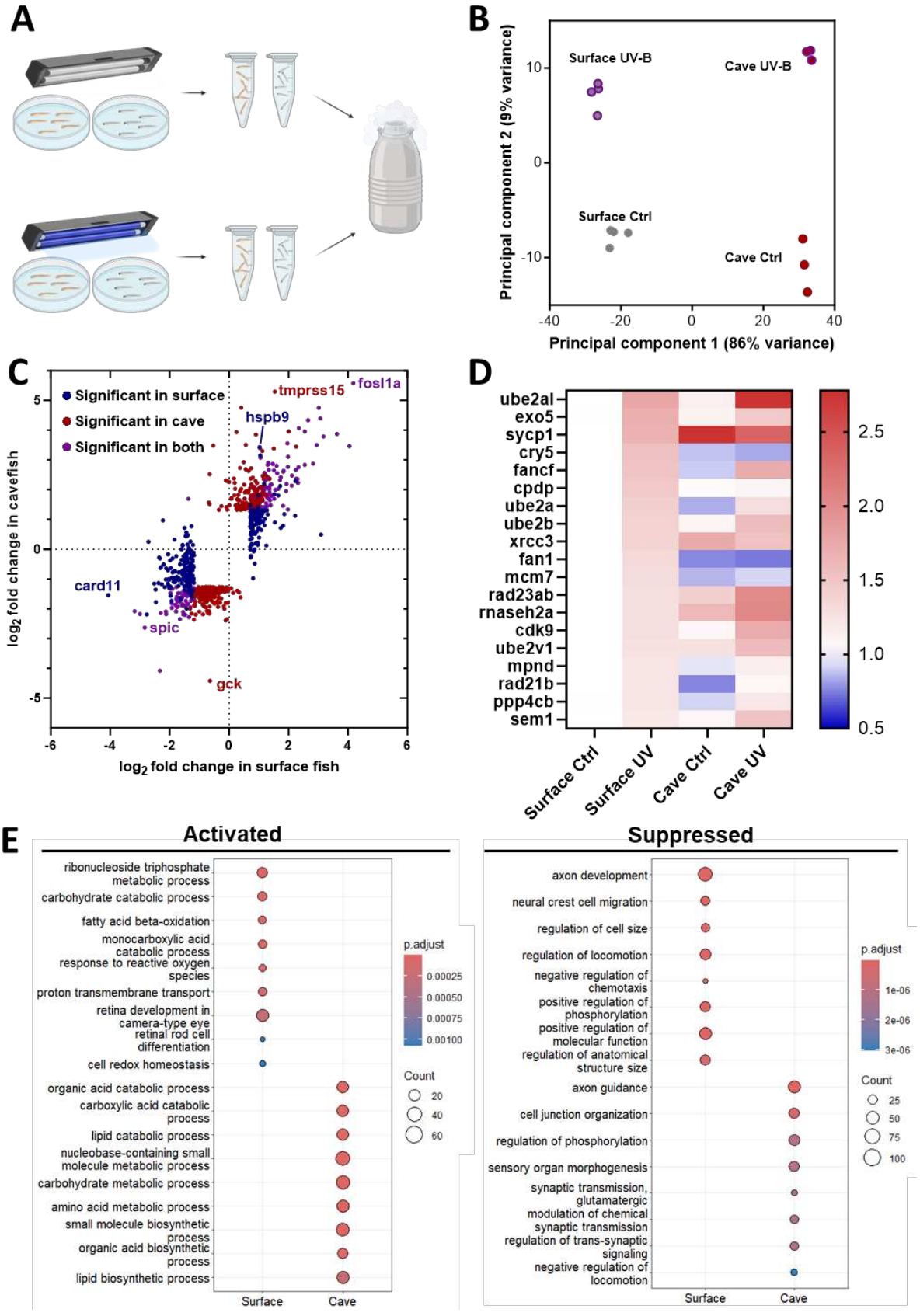

**Figure 3. Transcriptional responses to UV-B-induced DNA damage in surface fish and cavefish.** **(A)** Schematic of experimental design. **(B)** Multidimensional scaling plot depicting the variances in principal component space between the processed sequencing samples. PC1 (two-way ANOVA: (Treatment) $F_{1,10}$=6.388, $p$=0.03, (Population) $F_{1,10}$=4970, $p$<0.0001, (Interaction) $F_{1,10}$=17.56, $p$=0.0019. PC2 (two-way ANOVA: (Treatment) $F_{1,10}$=465.0, $p$<0.0001, (Population) $F_{1,10}$=0.4969, $p$=0.497, (Interaction) $F_{1,10}$=18.56, $p$=0.0015 **(C)** Bi-directional volcano plot of changes in gene expression in surface and cave larvae after exposure to DNA damaging UV-B radiation. **(D)** Heat map of gene expression in DNA repair genes which responded significantly in UV-B-exposed surface fish.

To assess whether a similar level of DNA damage in the different cell lines results in variations in DNA damage repair, we quantified γH2AX levels after UV treatment. Measurements were taken bi-hourly for 6 hours post exposure. The surface fish cells demonstrated a marked increase in γH2AX, whereas the cavefish cell lines showed only a modest rise, implying a diminished UV damage repair capability in cavefish cells (Fig 4C and 4D). To validate these results, we repeated these experiments on liver-derived cell lines [39] and observed a similar trend of reduced levels of γH2AX after radiation exposure in cavefish-derived cells, while the surface fish cells showed strong induction (Fig S4D). This pattern suggests that the DDR differences are not confined to tissue type. To directly test the ability to repair DNA, we employed a host cell reactivation assay [42,43]. Briefly, green fluorescent protein (GFP) plasmid was treated with 600 J/m$^2$ UV. We transfected the cell lines with either an intact or the *in vitro* UV damaged GFP plasmid and tracked GFP fluorescence recovery after 50 hours using flow cytometry as a proxy for the ability of the host cell to repair the plasmid (Fig 4G). Consistent with the γH2AX findings, the UV-damaged plasmid transfected cavefish cells displayed a substantially lower GFP signal recovery (~22% relative to control) than the surface fish cells (~49% relative to control) (Fig 4E and 4F). These observations, indicating a diminished DNA repair capacity, align with the sleep behavior differences we observed in UV-treated fish larvae.

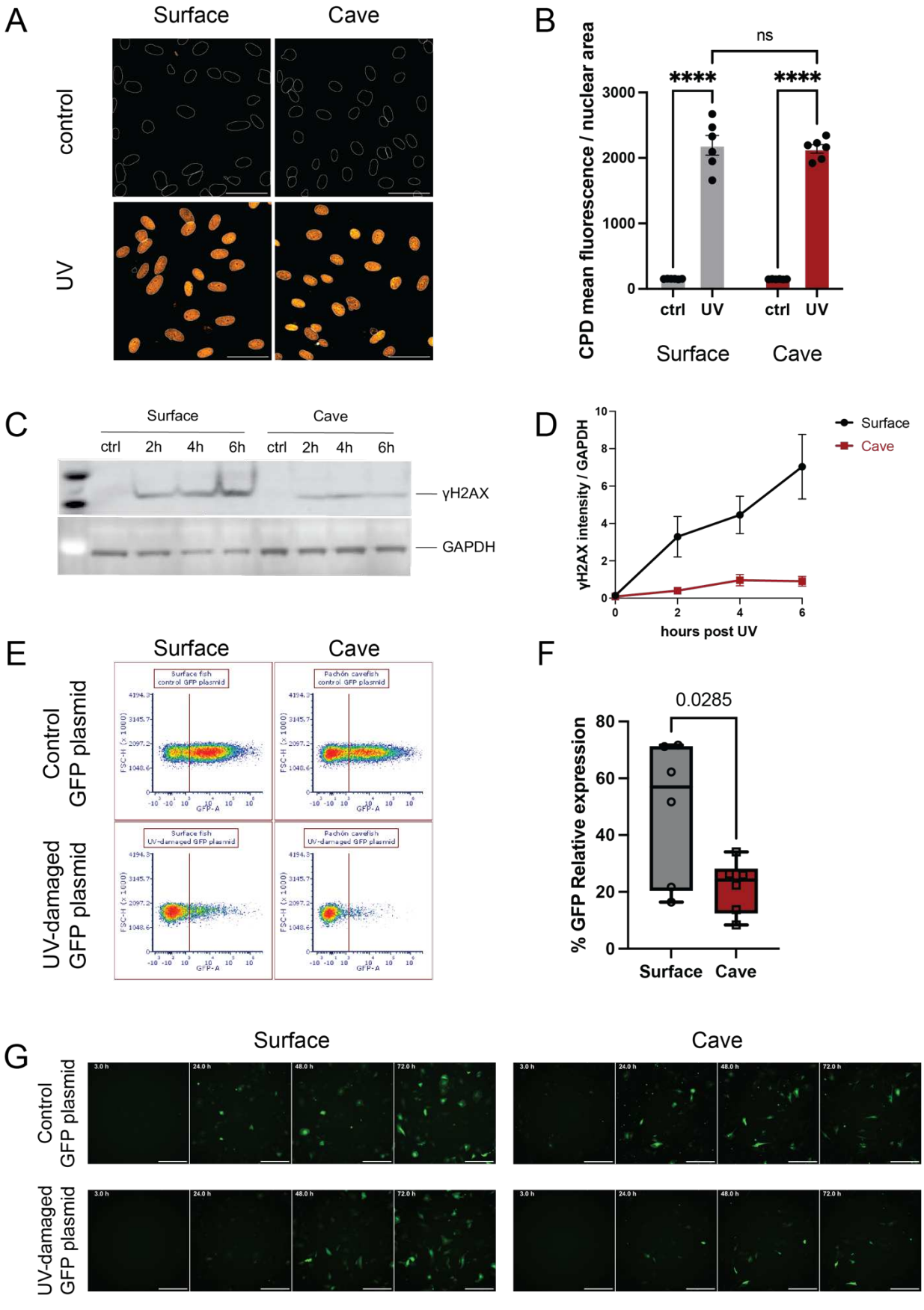

**Figure 4.** Pachón cavefish-derived cells exhibit a lower UV-induced DNA damage response and repair compared to surface fish. **(A,B)** Immunostaining of CPD shows a similar DNA damage level induced by UV in surface fish and Pachón cavefish embryonic fibroblasts. White circles indicate the nuclear area by DAPI staining. Orange indicates CPD. Scale bar, 40 μm. *P*-values were determined by two-way ANOVA: $F = 0.09703$, $p = 0.7586$. ns $p = 0.6404$, **** $p < 0.0001$. **(C,D)** Western blot of γH2AX indicates a diminished DNA damage response in Pachón cavefish embryonic fibroblast compared to surface fish cells. **(E,F)** Flow cytometry images and quantification for host cell reactivation assays in surface fish and Pachón cavefish embryonic fibroblast. Red line sets the GFP positive signal threshold. *P*-values were determined by unpaired *t*-test. **(G)** Representative GFP images for host cell reactivation assays in surface fish and Pachón cavefish embryonic fibroblast. Scale bars, 500 μm.

DNA damage in the brain, ROS in the gut, and sleep loss are associated with aging [31,44,45]. While *A. mexicanus* cavefish have evolved many traits that would be detrimental to humans or other species there is evidence that they have also evolved metabolic and physiological resilience, enabling them to enjoy a similar or even extended lifespan compared to surface fish [32,46,47]. To examine the effects of long-term accumulation of DNA damage in the brain, elevated gut ROS, and sleep loss, we examined the transcriptional profiles of tissue in young and aged fish. Briefly, we dissected the brain, gut, liver, muscle, and heart of young (~1 year old) and aged (7–8 year old) surface fish and Pachón cavefish. PCA analysis for brain samples revealed a strong contribution of population to the sample variance, with samples separated by population across PC1 and accounting for 51% of the variance (Fig 5A). Interestingly, while surface fish samples were separated by age across PC2, there was no separation of samples by age in cavefish (Fig 5A). The same trend held true for gene expression in the gut (Fig S5A). PCA plots of gene expression in the heart and liver did not show clear separation across either population or age, while muscle tissue showed separation by population, but not age (Fig S5B–D). To examine the impacts on the broader transcriptome, we compared the number of differentially expressed genes between young and aged populations of surface fish and cavefish. Across all tissues, there were markedly more transcripts that were differentially expressed between young and aged surface fish than cavefish in the brain, gut, heart, liver, and muscle (Fig 5B). Together, these findings reveal that the transcriptome of cavefish is resilient to age-associated changes despite sleep loss, elevated ROS, and elevated DNA damage.

We sought to examine the specific genes that were differentially expressed between surface fish and cavefish, providing potential mechanisms of resilience to DNA damage and sleep loss. Because sleep is considered necessary, specifically for repair of neuronal DNA damage, we first examined transcriptional differences in the aging surface fish and cavefish brains. Within the brain, there were only five genes which showed significant changes in both surface fish and cavefish; among these was the gene *top2a*, which is reduced in both populations (Fig 5C). *Top2a*

is considered essential for structural maintenance of chromosomes during cell division. Intriguingly, GSEA analysis did not reveal any significantly enriched pathways in aged surface fish brains despite the high number of differentially regulated genes, while the aged cavefish brains showed suppression of gene sets related to chromosome condensation and segregation (Fig 5D). These processes are known to deteriorate with age as a consequence of unrepaired DNA damage, particularly in the brain [48]. Across non-brain tissues, we found enrichment for a wide variety of processes, some which overlapped across tissues and populations and some which did not, consistent with the idea that aging is a complex process governed by many factors (Fig S6). Taken together, these results indicate that, despite elevated levels of DNA damage and impaired DNA damage and repair mechanisms, cavefish are at least partially protected from their harmful effects, and exhibit reduced transcriptional changes during aging.

## Discussion

We have investigated differences in DNA damage and the DDR pathway in *A. mexicanus,* a model for evolved sleep loss. UV and other agents that induce DNA damage promote sleep in diverse animals, suggesting a fundamental and highly conserved relationship between DNA damage and sleep regulation [10,35,49]. Similarly, we find that DNA damage in the brain and ROS levels in the gut are elevated in Pachón cavefish compared to surface fish. These findings are consistent with the phenotypes of sleep-deprived invertebrates and mammals, supporting the notion that cavefish are sleep deprived[11,35]. Beyond the Pachón cavefish population, all three other cavefish populations have been found to have reduced sleep (Cite). Further investigation of DNA damage in these populations is necessary to determine whether the cellular effects of sleep loss are conserved in independently evolved cavefish populations[28,50]. There are many species that have evolved sleep loss, particularly in defined ecological contexts, including newborn cetaceans that forgo sleep, the Arctic tern that suppresses sleep during the mating season, and frigate birds that have reduced and unilateral sleep during prolonged flight[51–53]. It will be highly informative to investigate the presence of DNA damage and other markers of sleep loss within a natural ecological context and in evolutionary models with altered sleep.

Our cellular analysis further revealed a muted DDR in cavefish, which likely contributes to the increased DNA damage noted *in vivo*. Since photolyases are primarily utilized for the repair of UV-induced cyclobutene pyrimidine dimers, and their repair processes are also dependent on light input [54], it is plausible that these genes were not favored by natural selection in cavefish, leading to accumulated mutations and a loss of functional DNA damage response. This

hypothesis is supported by findings that Somalian cavefish have lost critical DNA repair enhancers needed for an induced DDR [55]. The fact that Mexican cavefish retain some capacity for light-induced DNA repair might be attributed to their relatively recent divergence from their surface-dwelling counterparts, estimated to be less than 200,000 years ago [56,57]. Although our findings are consistent with studies on DNA repair in other cavefish species, they contrast with previous research suggesting an increased DNA repair function in certain *Astyanax* cavefish populations [29]. While increased expression of DNA repair genes is also observed in our study (Fig S3), our cellular assays demonstrate that this does not equate to enhanced DNA repair activity. However, our analysis focused only on two different cell lines (embryonic fibroblasts and liver-derived cells), while the previous study looked at DNA repair in fins [29]. Further research will be required to resolve these differences and fully understand DNA repair dynamics in cavefish.

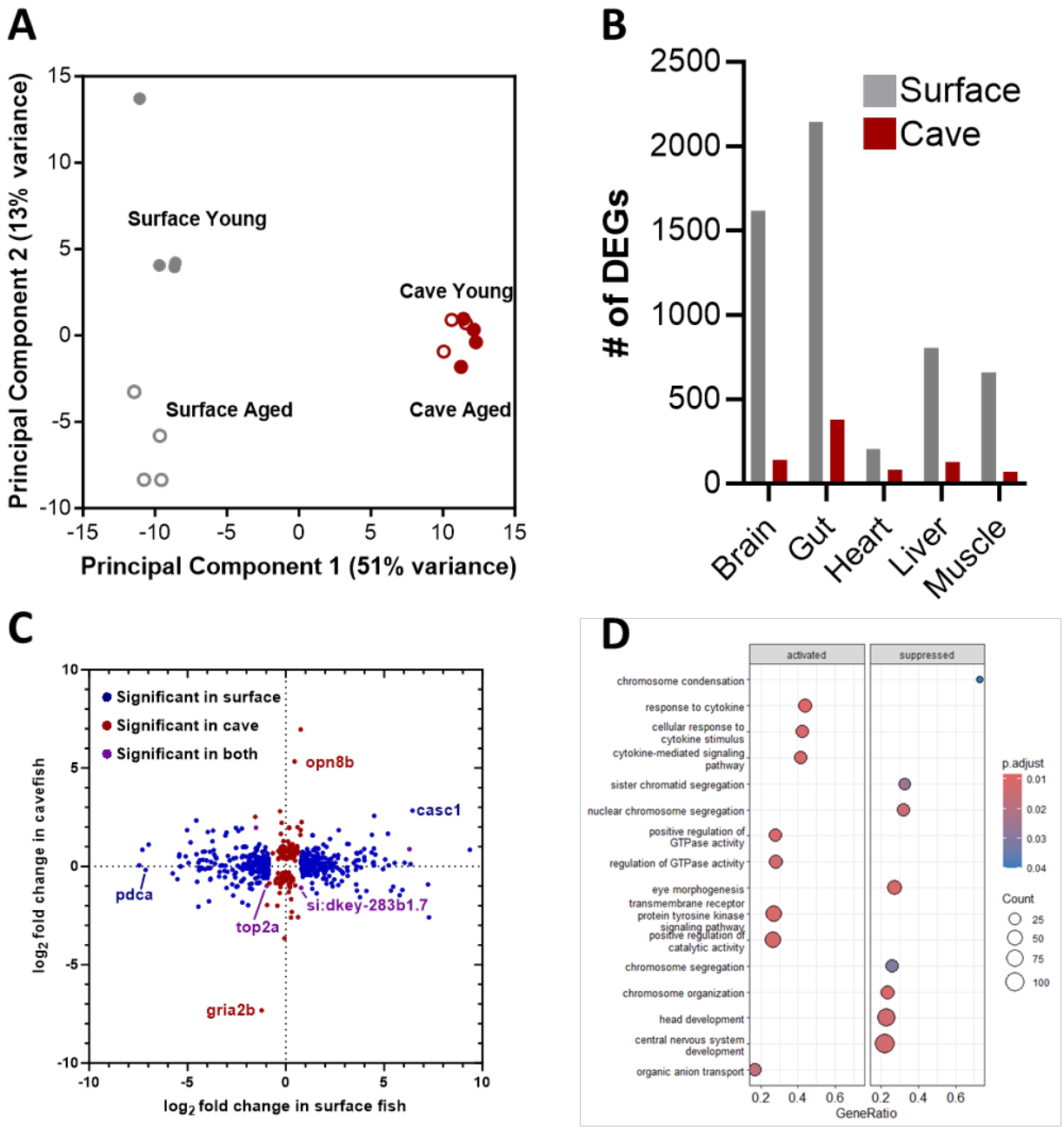


**Figure 5. Transcriptional response to aging is diminished in cavefish across tissues. (A)** Multidimensional scaling plot plotting the distances in principal component space between the brain samples. PC1 (two-way ANOVA: (Treatment) $F_{1,11}$=4.209, $p$=0.0648, (Population) $F_{1,11}$=2133, $p$<0.0001, (Interaction) $F_{1,11}$=0.029, $p$=0.867 PC2 (two-way ANOVA: (Treatment) $F_{1,11}$=16.83, $p$=0.0018, (Population) $F_{1,11}$=0.0002, $p$<0.99, (Interaction) $F_{1,11}$=19.37, $p$=0.0011 **(B)** Number of differentially expressed genes in the aged condition across tissues. **(C)** Bi-directional volcano plot depicting differences in gene expression between young and aged brains. **(D)** Dot plot visualizing the top 8 activated and suppressed gene ontology terms in aged cavefish brains resulting from GSE analysis.

In *Drosophil*a and mice, both acute and chronic sleep loss is associated with reduced longevity,

and it is postulated that ROS-associated gut dysregulation leads to death in chronically sleep-deprived individuals[11]. Therefore, it is interesting that cavefish do not exhibit clear signs of accelerated aging compared to surface fish [32,58]. The lifespan of surface and cave populations of *A. mexicanus* is reported to exceed 20 years, largely preventing the use of longevity as a readout for aging (Rohner, personal communication). However, DNA damage and aging-associated transcriptional changes can provide a proxy for biological aging. The findings that the transcriptional architecture of cavefish does not vary to the degree of surface fish indicates a form of genomic stability or a decelerated aging process, which could be a focal point for future research into the mechanics of aging and its relationship with sleep and DNA repair. In addition to sleep loss, cavefish have fatty livers, reductions in heart regeneration, and chronically elevated blood glucose [32,59]. These findings raise the possibility that cavefish may have evolved a broad range of resilience mechanisms to biological stress. Consistent with this notion, cavefish have evolved a reduced metabolic rate and elevated metabolites associated with hypoxia and longevity [58]. Many of these features, such as reduced metabolic rate, are present in other long-lived organisms, including the naked mole-rat (*Heterocephalus glaber*) and the cave olm (*Proteus anguinus*) [46]. Comparing differences between surface fish and cavefish, or similarities between cavefish and other long-lived models, may provide a system to study resilience to biological stress.

Taken together, these findings suggest that cavefish can be used as a model to study evolved loss of DDR and biological resilience. Growing genetic and genomic tools in cavefish including multiple chromosome-level sequenced genomes and single-cell RNA sequencing atlases may allow for the identification of markers of selection for DNA repair and cell-type specific transcriptional changes in sleep-regulating neurons. In addition, the study of DNA damage and ROS in additional populations of cavefish provides the opportunity to identify multiple mechanisms of DNA damage response.

## Material and Methods

### Fish Husbandry

Fish used in behavioral, immunohistochemistry, and UV-B experiments were generated and raised at Texas A&M University in dedicated aquarium facilities, with water temperature maintained at 23°C on a 14 hour light : 10 hour dark schedule as previously described [60]. To stimulate breeding, water temperature was raised by ~2°C with a submersible heater, and fish

were fed frozen blood worms to satiation 2–3 times daily[61]. Following breeding, embryos were collected from tanks and raised in a temperature-controlled incubator under the same temperature and light cycle until used for experiments. Fish used for tissue dissections were collected from aquarium facilities at Florida Atlantic University, maintained under the same conditions. Fish and embryos used for cell line derivation were collected from the cavefish facility at the Stowers Institute for Medical Research, maintained under similar conditions, except for the food. Adult fish were fed with Mysis shrimp once in the morning and Gemma 800 (Skretting, Gemma Silk) once in the afternoon. Fish in the breeding cycle were fed with Gemma 800 once at noon.

Fibroblast cell line derivation

Embryos were collected after spawning and were dechorionated before 14 hours post fertilization (hpf). Embryos were then washed in washing media (PBS supplemented with 50 U/ml Penicillin + 0.05 mg/ml Streptomycin) for 30 min three times. Five embryos were transferred to a sterile 1.5 ml tube with 0.5 ml of wash media where the yolk sac of embryos was removed by pipetting up and down ~10 times with a 200 µl pipette tip. Tissues in 1.5 ml tubes were then centrifuged at 1200 g for 2 min at room temperature (RT) and the supernatant was discarded carefully. Next, 300 µl of TrypLE (Thermo Fisher Scientific, #12604021) was added to each 1.5 ml tube and incubated at 28°C for 5 min in a thermomixer at 800 g. Once the embryos were dissociated, embryo tissues were pipetted up and down several times, followed by centrifugation at 1200 g for 4 min. Cell pellets were resuspended in 400 µl growth media containing 15% fetal bovine serum (FBS) (Cytiva, #SH30071.02E), 0.8 mM calcium chloride, 1 µg/ml human insulin solution (Sigma, #I9278), and 1X L-Glutamine (Thermo Fisher Scientific, #25030081) in L-15 (Corning, #10-045-CV), and transferred to 1 well of a 48 well plate coated with 0.1% gelatin in advance. Cells were maintained and incubated with growth media in the incubator at 28°C without $CO_2$ and were observed every day with media changes 3 times per week (400 µl per well). Cells usually reached confluency 7–10 days after derivation. Cells were passaged once a week at a 1:4 to 1:10 ratio and expanded for cryopreservation in freezing media (90% FBS + 10% DMSO) at $2 \times 10^6$ per vial.

Host cell reactivation (HCR) assay

Experiments were designed and protocols were modified based on two previous studies [43,62]. An amount of 25 µl of pmaxGFP plasmid from Lonza Amaxa cell Nucleofector Kit V (Lonza, #VCA-1003) at a concentration of ~0.2 µg/µl was aliquoted into a 10 cm plate and irradiated with 600 J/$m^2$ of UV-C light with the lid open. The same batch of UV-treated plasmids was used for testing

all species to avoid batch-to-batch variation. Next, $1.2 \times 10^6$ cells were co-transfected with 6 µg of treated or untreated pmaxGFP. For each reaction, 82 µl base media and 18 µl of supplement was used to make the Nucleofector® Solution. Cell pellets were resuspended carefully in 100 µl RT Nucleofector® Solution per sample with 5 µg treated or untreated pmaxGFP added, then transferred into a certified cuvette. It was necessary for the samples to cover the bottom of the cuvette without air bubbles. Transfections were carried out with program T-027 using Amaxa Nucleofector II. Cuvettes were taken out of the holder once the program was finished. An amount of 20 µl of the mixture was added to 24-well plates with 1 ml of cell media and imaged every 1.5 hours for 3 days using a Nikon ECLIPSE Ti2 microscope with a 10X lens; the rest of the cells were added to 6-well plates with 3 ml of cell media for flow cytometry analysis.

Flow cytometry

Cells were harvested 50 hours post-transfection. The cell pellet collected from each well of a 6-well plate was resuspended in 500 µl 1X PBS. An amount of 1 µl of Ghost Dye solution (Cytek Bioscience, #13-0865-T100) was added to each 500 µl cell suspension, vortexed immediately, and was then incubated for 30 min at 2–8°C protected from light. After incubation, the cell suspension was spun at 400 g for 5 min at RT and the supernatant was discarded. Next, 500 µl media was added to the cell pellets to prepare for flow cytometry using Cytek Aurora. The %GFP relative expression (%RE) was calculated using $F = N \times MFI/S$, where N is the total number of live cells appearing in the positive region for GFP, MFI is the mean fluorescence intensity of the N cells, and S is the total number of live cells; $\%RE = F_t/F_u$, where $F_t$ is the F of cells transfected with treated plasmids and $F_u$ is the F of cells transfected with undamaged plasmids. Live cells were identified based on altered forward and side scatters.

Immunohistochemistry

For immunostaining in fish, larvae aged 6 dpf were fixed at ZT1 in a 1X Phosphate Buffer Solution (PBS) with 4% Paraformaldehyde and 0.1% Tween 20 for 6 hours on ice as previously described [63,64]. After fixation, samples were rinsed 3 times in PBS with 0.1% Tween 20 (PBT) at RT, with 10 min between rinses. Samples were incubated overnight at 4°C in 1:500 anti-γH2AX (Genetex, #GTX127342) with 0.1% PBT and 2% Bovine Serum Albumin (BSA). After overnight incubation, samples were rinsed 3 times in 0.1% PBT at RT, with 10 min between rinses. Next, samples were incubated in 1:500 Goat anti-rabbit 488 (Abcam, #ab150077) and 1 µg/ml DAPI (Thermo Fisher Scientific, #D1306) in 0.1% PBT. Finally, samples were rinsed again 3 times in 0.1% PBT at RT

with 10 min between rinses, stored overnight at 4°C, and then imaged on a Nikon A1 confocal microscope with a 20X water immersion lens.

For vimentin staining in cell culture, cells were fixed with 4% Paraformaldehyde in PBS for 15 min at RT. After fixation, cells were rinsed 3 times in PBS at RT, with 5 min between rinses. After fixation, cells can be stored for up to 1 week at 4°C. Fixed cells were permeabilized with 0.1% Triton in PBS for 30 min at RT, then blocked with 20% FBS diluted in 0.1% PBT for 1 hour at RT. Samples were then incubated overnight at 4°C with 1:200 anti-vimentin antibody (Sigma, #V5255) in blocking buffer. After overnight incubation, samples were rinsed 3 times in 0.1% PBT at RT with 5 min between rinses. Next, samples were incubated for 1 hour at room temperature in darkness with 1:300 Donkey Anti-Mouse IgG (H+L) 568 (Biotium, #20105) and 1 µg/ml DAPI (Sigma, #10236276001) in 5% FBS and 0.1% PBT. Finally, samples were rinsed again 3 times in 0.1% PBT with 5 min between rinses, rinsed once with PBS, stored overnight at 4°C, and then imaged on a Nikon ECLIPSE Ti2 confocal microscope with a 40X water immersion lens.

For CPD staining in cell culture, cells were plated at $2 \times 10^5$ per well in a glass bottom dish (Cellvis, #D35C4-20-1.5-N) 2 days before the experiment. Cells were washed once with PBS and cell media was removed before exposure to 100 J/m$^2$ UV-C (Stratalinker® UV Crosslinker, Model 2400, #400075). Cells were fixed 5 min after UV-C treatment using 4% Paraformaldehyde in PBS for 15 min at RT. After fixation, cells were rinsed 3 times in PBS at RT with 5 min between rinses. After fixation, cells can be stored up to 1 week at 4°C. Fixed cells were permeabilized with 0.1% Triton in PBS for 30 min at RT, followed by 2 rinses in PBS with 5 min between rinses. Next, 2M Hydrochloric acid (HCl) was used to denature cellular DNA for 30 min at RT, followed by 5 rinses in 0.1% PBT with 5 min between rinses. After this, cells were blocked with 20% FBS diluted in 0.1% PBT for 1 hour at RT. Samples were then incubated overnight at 4°C with 1:1000 anti-CPD antibody (TDM-2, Cosmo Bio, #CAC-NM-DND-001) in blocking buffer. After overnight incubation, samples were rinsed 3 times in 0.1% PBT at RT with 5 min between rinses. Next, samples were incubated for 1 hour in darkness with 1:300 Donkey Anti-Mouse IgG (H+L) 568 (Biotium, #20105) and 1 µg/ml DAPI (Sigma, #10236276001) in 5% FBS and 0.1% PBT. Finally, samples were rinsed again 3 times in 0.1% PBT with 5 min between rinses, rinsed once with PBS, stored overnight at 4°C, and then imaged on a Nikon ECLIPSE Ti2 confocal microscope with a 40X water immersion lens.

Western Blot analysis

Fish fibroblast cells and liver-derived cells [39] were plated at $5 \times 10^4$ per well in 6-well plates 4 days before the experiment. Cell media was removed before cells were exposed to 3000 J/m$^2$ UV-C. Fresh cell growth media was added to the cells and incubated for 2, 4, or 6 hours. Lysis buffer was made with 1X protease inhibitor (25X stock, Sigma, #11873580001) and 1X phosphatase inhibitor (100X stock, Cell Signaling, #5870S) in RIPA buffer (Thermo Fisher Scientific, #89900). Next, 100 µl lysis buffer was added to each well and cells were detached by cell scraper (VWR INTERNATIONAL, #10062-904). Samples were fully lysed by pipetting up and down ~5 times with a fine needle syringe (BD Medical, #328438) and vortexed for 10 seconds. The supernatant was collected as protein fractions after two rounds of centrifugation at 12,000 g for 20 min at 4°C. Protein concentrations were determined by bicinchoninic acid (BCA) protein assay (Thermo Fisher Scientific, #23227).

Protein samples were loaded to the protein gel (Thermo Fisher Scientific, #NP0323BOX) at ~10–13 µg per lane. Protein gels were run in MOPS buffer (Thermo Fisher Scientific, #NP0001) at 130 V for 80 min, then transferred to PVDF membrane (Sigma, #IPVH00010) in 4°C at 215 mA for 50 min. PVDF membranes were blocked in blocking buffer (LI-COR, #927-80001) for an hour at RT, then incubated with primary antibody overnight at 4°C in 1:1000 anti-γH2AX (Genetex, #GTX127342) and 1:1000 anti-GAPDH (Proteintech, #60004-1-Ig) with blocking buffer. On the next day, PVDF membranes were washed 3 times in 0.1% TBST with 5 min between rinses and incubated with 1:10,000 Donkey anti-mouse (LI-COR, #926-32212) and anti-rabbit (LI-COR, #926-68073) secondary antibody at RT for an hour. Finally, samples were rinsed again 3 times in 0.1% TBST with 10 min between rinses, and then imaged and quantified on LI-COR Odyssey® CLx with Image Studio v5.2 software.

ROS imaging

ROS imaging was implemented based on previous protocols used in Drosophila[11]. Larvae aged 6 dpf were euthanized at ZT1 by immersion in ice-chilled aquarium water for 30 min. Following euthanasia, samples were incubated in 60 µM dihydroethidium (DHE; Thermo Fisher Scientific, D11347) for 5 min at RT, covered in foil to protect it from light. Next, samples were rinsed for 5 min in 1X PBS, then mounted in 2% low melting point agarose (Sigma-Aldrich, A9414) and the entire gut was imaged on a Nikon A1R confocal microscope with a 10X air objective, with a slice thickness of 4 µm. After interaction with superoxide radicals, DHE is converted into 2-hydroxy ethidium, which is optimally excited at 480 nm and fluoresces red (wavelength > 550 nm); therefore, the sample was excited with a 488 nm laser and imaged with a detector in the 570–616

nm range [65]. ROS in the gut was quantified by calculating a z-projection (calc: Average Intensity) in ImageJ (NIH, v1.54f) and manually drawing ROIs around anatomically defined regions of the gut [66].

Sleep Experiments

Sleep experiments used previously described methodology [67]. For induction of DNA damage, larvae aged 5 dpf were transferred to individual wells of a 24-well plate at ZT7–8 (VWR, 82050-892), and acclimated overnight to the testing environment. At ZT0 the next day, larvae were subjected to either 60 seconds of control white light or 30 or 60 seconds of UV-B light in a UV-Crosslinker cabinet (Spectro-UV, XL-1500) fitted with UV bulbs with a spectral peak at 315 nm (UV-B; Spectro-UV, BLE-1T158). Following treatment, well plates were immediately returned to the testing environment and filmed from above using a USB camera (Basler, acA1300-200) fitted with a 16 mm fixed focal length lens (Edmund Optics, 67-714) and an infrared pass filter (Edmund Optics, 65-796) to ensure consistent image quality after the day/night transition. Larvae were lit from below using infrared light strips (850 nm), diffused through a custom-made white acrylic light box (TAP Plastics).

Locomotor behavior was tracked in Ethovision XT (Noldus), and frame-by-frame velocity data was exported and analyzed using a custom Python script, with sleep defined as 60 seconds or more of consolidated immobility. A velocity cut-off of 6 mm/s was used to distinguish active swimming from passive drift.

RNA Extraction and Sequencing

For RNA sequencing on fish fibroblast cells, cells were detached with TrypLE and washed once with cell media. Cell pellets were collected after centrifugation at 1000 g for 5 min, snap frozen in liquid nitrogen, and stored at -80°C prior to RNA extraction. For UV RNA sequencing experiments, larvae were treated identically to the sleep experiments until 1.5 hours after UV exposure, at which point they were transferred to 1.5 ml centrifuge tubes, with 4 larvae pooled into each tube. The larvae were euthanized by chilling on ice before immediately proceeding to RNA extraction.

For RNA sequencing experiments on adults, dissections were performed at Florida Atlantic University. Briefly, tissue was dissected between ZT0 and ZT3 from at least 4 fish at each age and population group. Tissue was immediately flash frozen in liquid nitrogen. To extract RNA, 1 ml of TRIzol was added to each sample. Samples were homogenized, and then 200µl chloroform

was added to each tube, followed by vigorous shaking. Samples were incubated on ice for 15 min, then phase separated by centrifuging at 12,000 g for 15 min at 4°C. The resulting aqueous phase of the liquid was transferred to a fresh 1.5 ml tube, and then RNA was precipitated out by mixing with 0.5 ml isopropanol. Samples were incubated on ice for 10 min, then centrifuged at 12,000 g for 10 min at 4°C. The supernatant was removed by pouring and lightly shaking the tube, then the resulting pellet was washed by the addition of 1 ml 70% EtOH while vigorously flicking the tube. The samples were then centrifuged at 7500 g for 10 min at 4°C. The supernatant was removed by pouring and lightly shaking the tube, and the samples were air dried upside down for 10 min. Finally, the pellet was redissolved in 100ul of RNAse-free $H_2O$.

RNA Sequencing Data Analysis

Sample quality control, library preparation, and sequencing were performed by Novogene. Raw reads received from Novogene were mapped against the *Astyanax mexicanus* reference genome (version 2.0, GenBank Accession Number: GCA_000372685.2) using the splice-aware mapper STAR [68] to generate raw counts. Annotations were extracted from the *A. mexicanus* annotation file from Ensembl (Astyanax_mexicanus-2.0.108.gtf). Subsequent analysis was performed in RStudio (v4.3.0) using the differential expression testing software DESeq2 (v1.40.2) [69].

Data from the UV-B experiment and the aging experiment were analyzed using the same analysis pipeline, with each tissue type from the aging experiment analyzed separately. First, a DESeq object was created from the raw counts matrix and processed using the DESeq() command, which estimates size factors and dispersion, and fits the data to a negative binomial GLM. Normalized count values used in downstream analysis were generated using the counts() function (normalized = T). Sample variability for each group was visualized by first performing a variance stabilizing transformation using the vst() function, then generating a PCA plot from the resulting object with the plotPCA() function. To identify genes which were differentially expressed in response to UV-B treatment (or aging), each population treatment subset was reanalyzed as above, so that the effects of treatment on each population were considered separately. An adjusted $p$-value < 0.05 was used to determine a significant response to treatment.

Gene Ontology (GO) analysis

Gene ontology pathway analyses were performed using the clusterProfiler package (v4.8.3) in R. For gene set enrichment analyses, genes were first ranked according to the magnitude of their response; the ranking value was calculated as $-\log_{10}(\text{pval})/\text{sign}(\log_2 FC)$, to account for both

direction and magnitude of response. The resulting ranked list was processed using the gseGO() function (options: ont='BP'', keyType='SYMBOL', pvalueCutoff=0.05, OrgDB = org.Dr.eg.db, pAdjustMethod = 'BH'). For visualization purposes, similar GO terms were grouped together using the simplify() function (options:by='p.adjust', select_fun=min), and visualized using the dotplot() function. For the UV-B experiment, since there were many overlapping GO terms, the top 10 unique terms in each direction were plotted.

Quantitative PCR

Adult fins were collected at Zeitgeber or Circadian time 8. 5 dpf larvae were collected at Zeitgeber or Circadian time 2, 6, 10 and 14. Samples were then homogenized and total RNA extracted as above. cDNA was synthesized from 500 ng RNA using iScript cDNA synthesis kit (BIO-RAD, #1708891). Approximately 50 ng of cDNA was used for quantitative PCR (qPCR) using Perfecta SYBR Green with Low ROX (Quantabio, #95074-012) with a QuantStudio 5 Real-Time PCR System. Specificity of each amplicon and cDNA final concentration was optimized via analysis of post-reaction dissociation curves, validating a single amplicon for each set of primers. Analysis was conducted using the ΔΔCt method. All samples were run in 3-4 replicates and normalized to the housekeeping gene *rpl13a*. Primer sequences used are as follows:

*cpdp* (ENSAMXG00000001885): FW: 5'- GGCCTCTCCTAAGCTGGAGT -3'

RV: 5'- GTCCACAGGTGGGAATTCAG -3'

*ddb2* (ENSAMXG00000000525):

FW: 5'- AAGCTGCACAAAGCCAAAGT-3'

RV: 5'- AGACGATGTTGCCACTAGCC -3'.

*rpl13a* (ENSAMXG00000033532):

FW 5'- CGCAACAAATTGAAGTACCTG -3'

RV: 5'- GGTTCGTGTTCATCCTCTTG -3'

**Acknowledgements**

We would like to thank the help and support provided by facility cores at Stowers Institute; specifically, cavefish team for fish husbandry, KyeongMin Bae and Jose Emmanuel Javier for flow cytometry, and Di Wu for data analysis. This work was supported by the National Institute of Health R24OB030214 to WW, NR, and ACK and R21 NS122166 to ACK and US-Israel Binational Science Foundation Award 2021177 to ACK and LA.

## References


1. McNamara P, Barton R, Nunn C. Evolution of sleep: phylogenetic and functional perspectives. Cambridge. 2009. doi:10.1017/CBO9780511642074
2. Aulsebrook AE, Jones TM, Rattenborg NC, Roth TC, Lesku JA. Sleep Ecophysiology: Integrating Neuroscience and Ecology. Trends Ecol Evol. 2016;31: 590–599. doi:10.1016/j.tree.2016.05.004
3. Joiner WJ. Unraveling the Evolutionary Determinants of Sleep. Current Biology. 2016;26: R1073–R1087. doi:10.1016/j.cub.2016.08.068
4. Zimmerman JE, Naidoo N, Raizen DM, Pack AI. Conservation of sleep: insights from non-mammalian model systems. Trends in Neurosciences. 2008. pp. 371–376. doi:10.1016/j.tins.2008.05.001
5. Keene AC, Duboue ER. The origins and evolution of sleep. J Exp Biol. 2018. doi:10.1242/jeb.159533
6. Siegel JM. Clues to the functions of mammalian sleep. Nature. 2005;437: 1264–1271. doi:10.1038/nature04285
7. Frank MG. The Ontogenesis of Mammalian Sleep: Form and Function. Curr Sleep Med Rep. 2020;6: 267–279. doi:10.1007/s40675-020-00190-y
8. Hartmann EL. The Functions of Sleep. Yale University Press; 1973.
9. Zada D, Bronshtein I, Lerer-Goldshtein T, Garini Y, Appelbaum L. Sleep increases chromosome dynamics to enable reduction of accumulating DNA damage in single neurons. Nat Commun. 2019;10: 895. doi:10.1038/s41467-019-08806-w
10. Zada D, Sela Y, Matosevich N, Monsonego A, Lerer-Goldshtein T, Nir Y, et al. Parp1 promotes sleep, which enhances DNA repair in neurons. Mol Cell. 2021;81: 4979-4993.e7. doi:10.1016/j.molcel.2021.10.026
11. Vaccaro A, Kaplan Dor Y, Nambara K, Pollina EA, Lin C, Greenberg ME, et al. Sleep Loss Can Cause Death through Accumulation of Reactive Oxygen Species in the Gut. Cell. 2020;181: 1307-1328.e15. doi:10.1016/j.cell.2020.04.049
12. Carroll JE, Cole SW, Seeman TE, Breen EC, Witarama T, Arevalo JMG, et al. Partial sleep deprivation activates the DNA damage response (DDR) and the senescence-associated secretory phenotype (SASP) in aged adult humans. Brain Behav Immun. 2016;51: 223–229. doi:10.1016/j.bbi.2015.08.024
13. Bellesi M, Bushey D, Chini M, Tononi G, Cirelli C. Contribution of sleep to the repair of neuronal DNA double-strand breaks: evidence from flies and mice. Sci Rep. 2016;6: 36804. doi:10.1038/srep36804
14. Goetting DL, Mansfield R, Soto R, Buskirk C Van. Cellular damage, including wounding, drives C. elegans stress-induced sleep. J Neurogenet. 2020;34: 430–439. doi:10.1080/01677063.2020.1752203
15. Cheung V, Yuen VM, Wong GTC, Choi SW. The effect of sleep deprivation and disruption on DNA damage and health of doctors. Anaesthesia. 2019;74: 434–440. doi:10.1111/anae.14533
16. Haynes PR, Pyfrom ES, Li Y, Stein C, Cuddapah VA, Jacobs JA, et al. A neuron-glia lipid metabolic cycle couples daily sleep to mitochondrial homeostasis. Nat Neurosci. 2024;27: 666–678. doi:10.1038/s41593-023-01568-1

17. Cirelli C. The genetic and molecular regulation of sleep: from fruit flies to humans. Nat Rev Neurosci. 2009;10: 549–560. doi:10.1038/nrn2683
18. Allada R, Siegel JM. Unearthing the phylogenetic roots of sleep. Curr Biol. 2008;18: R670–R679. doi:10.1016/j.cub.2008.06.033
19. Keene A, Yoshizawa M, McGaugh S. Biology and Evolution of the Mexican Cavefish. 1st Editio. New York: Academic Press; 2015.
20. Kowalko J. Utilizing the blind cavefish Astyanax mexicanus to understand the genetic basis of behavioral evolution. J Exp Biol. 2020;223. doi:10.1242/JEB.208835
21. McGaugh SE, Kowalko JE, Duboué E, Lewis P, Franz-Odendaal TA, Rohner N, et al. Dark world rises: The emergence of cavefish as a model for the study of evolution, development, behavior, and disease. J Exp Zool B Mol Dev Evol. 2020;334: 397–404. doi:10.1002/jez.b.22978
22. Yoshizawa M. Behaviors of cavefish offer insight into developmental evolution. Mol Reprod Dev. 2015;82: 268–280. doi:10.1002/mrd.22471
23. Keene AC, Appelbaum L. Sleep in Fish Models. Handbook of Behavioral Neuroscience. 2019. doi:10.1016/B978-0-12-813743-7.00024-4
24. Duboué ER, Keene AC, Borowsky RL. Evolutionary convergence on sleep loss in cavefish populations. Curr Biol. 2011;21: 671–676. doi:10.1016/j.cub.2011.03.020
25. Aspiras A, Rohner N, Marineau B, Borowsky R, Tabin J. Melanocortin 4 receptor mutations contribute to the adaptation of cavefish to nutrient-poor conditions. Proceedings of the National Academy of Sciences. 2015;112: 9688–73.
26. Duboué ER, Keene AC, Borowsky RL. Evolutionary convergence on sleep loss in cavefish populations. Current Biology. 2011;21: 671–676. doi:10.1016/j.cub.2011.03.020
27. Mack KL, Jaggard JB, Persons JL, Roback EY, Passow CN, Stanhope BA, et al. Repeated evolution of circadian clock dysregulation in cavefish populations. PLoS Genet. 2021;17: 1–32. doi:10.1371/journal.pgen.1009642
28. Yoshizawa M, Robinson BG, Duboué ER, Masek P, Jaggard JBJ, O'Quin KEK, et al. Distinct genetic architecture underlies the emergence of sleep loss and prey-seeking behavior in the Mexican cavefish. BMC Biol. 2015;20: 15. doi:10.1186/s12915-015-0119-3
29. Beale A, Guibal C, Tamai TK, Klotz L, Cowen S, Peyric E, et al. Circadian rhythms in Mexican blind cavefish Astyanax mexicanus in the lab and in the field. Nat Commun. 2013;4: 2769. doi:10.1038/ncomms3769
30. Arble DMDM, Bass J, Behn CDCD, Butler MPMP, Challet E, Czeisler C, et al. Impact of Sleep and Circadian Disruption on Energy Balance and Diabetes : A Summary of Workshop Discussions. Sleep. 2015;38: 1849–1860. doi:10.5665/sleep.5226
31. Carroll JE, Prather AA. Sleep and biological aging: A short review. Curr Opin Endocr Metab Res. 2021;18: 159–164. doi:10.1016/j.coemr.2021.03.021
32. Riddle MR, Aspiras AC, Gaudenz K, Peuß R, Sung JY, Martineau B, et al. Insulin resistance in cavefish as an adaptation to a nutrient-limited environment. Nature. 2018;555: 647–651. doi:10.1038/nature26136
33. Cobham AE, Rohner N. Unraveling stress resilience: Insights from adaptations to extreme environments by Astyanax mexicanus cavefish. J Exp Zool B Mol Dev Evol. 2024. doi:10.1002/jez.b.23238

34. Rohner N. Cavefish as an evolutionary mutant model system for human disease. Dev Biol. 2018;441: 355–357. doi:10.1016/j.ydbio.2018.04.013
35. Bellesi M, Bushey D, Chini M, Tononi G, Cirelli C. Contribution of sleep to the repair of neuronal DNA double-strand breaks: evidence from flies and mice. Sci Rep. 2016;6: 36804. doi:10.1038/srep36804
36. Siddiqui MS, François M, Fenech MF, Leifert WR. Persistent γH2AX: A promising molecular marker of DNA damage and aging. Mutat Res Rev Mutat Res. 2015;766: 1–19. doi:10.1016/j.mrrev.2015.07.001
37. Öztürk-Çolak A, Inami S, Buchler JR, McClanahan PD, Cruz A, Fang-Yen C, et al. Sleep Induction by Mechanosensory Stimulation in Drosophila. Cell Rep. 2020;33: 108462. doi:10.1016/j.celrep.2020.108462
38. Satelli A, Li S. Vimentin in cancer and its potential as a molecular target for cancer therapy. Cell Mol Life Sci. 2011;68: 3033–46. doi:10.1007/s00018-011-0735-1
39. Krishnan J, Wang Y, Kenzior O, Hassan H, Olsen L, Tsuchiya D, et al. Liver-derived cell lines from cavefish Astyanax mexicanus as an in vitro model for studying metabolic adaptation. Sci Rep. 2022;12: 10115. doi:10.1038/s41598-022-14507-0
40. Wang B, Wu L, Li D, Liu Y, Guo J, Li C, et al. Induction of Pluripotent Stem Cells from Mouse Embryonic Fibroblasts by Jdp2-Jhdm1b-Mkk6-Glis1-Nanog-Essrb-Sall4. Cell Rep. 2019;27: 3473-3485.e5. doi:10.1016/j.celrep.2019.05.068
41. Stringer C, Wang T, Michaelos M, Pachitariu M. Cellpose: a generalist algorithm for cellular segmentation. Nat Methods. 2021;18: 100–106. doi:10.1038/s41592-020-01018-x
42. Nagel ZD, Margulies CM, Chaim IA, McRee SK, Mazzucato P, Ahmad A, et al. Multiplexed DNA repair assays for multiple lesions and multiple doses via transcription inhibition and transcriptional mutagenesis. Proc Natl Acad Sci U S A. 2014;111: E1823-32. doi:10.1073/pnas.1401182111
43. Tian X, Firsanov D, Zhang Z, Cheng Y, Luo L, Tombline G, et al. SIRT6 Is Responsible for More Efficient DNA Double-Strand Break Repair in Long-Lived Species. Cell. 2019;177: 622-638.e22. doi:10.1016/j.cell.2019.03.043
44. Maynard S, Fang EF, Scheibye-Knudsen M, Croteau DL, Bohr VA. DNA Damage, DNA Repair, Aging, and Neurodegeneration. Cold Spring Harb Perspect Med. 2015;5: a025130. doi:10.1101/cshperspect.a025130
45. Schumacher B, Pothof J, Vijg J, Hoeijmakers JHJ. The central role of DNA damage in the ageing process. Nature. 2021;592: 695–703. doi:10.1038/s41586-021-03307-7
46. Lunghi E, Bilandžija H. Longevity in Cave Animals. Front Ecol Evol. 2022;10. doi:10.3389/fevo.2022.874123
47. Medley JK, Persons J, Biswas T, Olsen L, Peuß R, Krishnan J, et al. The metabolome of Mexican cavefish shows a convergent signature highlighting sugar, antioxidant, and Ageing-Related metabolites. Elife. 2022;11. doi:10.7554/eLife.74539
48. Barroso-Vilares M, Macedo JC, Reis M, Warren JD, Compton D, Logarinho E. Small-molecule inhibition of aging-associated chromosomal instability delays cellular senescence. EMBO Rep. 2020;21: e49248. doi:10.15252/embr.201949248

49. DeBardeleben HK, Lopes LE, Nessel MP, Raizen DM. Stress-Induced Sleep After Exposure to Ultraviolet Light Is Promoted by p53 in Caenorhabditis elegans. Genetics. 2017;207: 571–582. doi:10.1534/genetics.117.300070
50. Moran RL, Jaggard JB, Roback EY, Kenzior A, Rohner N, Kowalko JE, et al. Hybridization underlies localized trait evolution in cavefish. iScience. 2022;25: 103778. doi:10.1016/j.isci.2022.103778
51. Lyamin O, Pryaslova J, Lance V, Siegel J. Animal behaviour: continuous activity in cetaceans after birth. Nature. 2005;435: 1177. doi:10.1038/4351177a
52. Rattenborg NC, Voirin B, Cruz SM, Tisdale R, Dell'Omo G, Lipp H-P, et al. Evidence that birds sleep in mid-flight. Nat Commun. 2016;7: 12468. doi:10.1038/ncomms12468
53. Lesku JA, Rattenborg NC, Valcu M, Vyssotski AL, Kuhn S, Kuemmeth F, et al. Adaptive sleep loss in polygynous pectoral sandpipers. Science. 2012;337: 1654–8. doi:10.1126/science.1220939
54. Liu Z, Tan C, Guo X, Kao Y-T, Li J, Wang L, et al. Dynamics and mechanism of cyclobutane pyrimidine dimer repair by DNA photolyase. Proc Natl Acad Sci U S A. 2011;108: 14831–6. doi:10.1073/pnas.1110927108
55. Zhao H, Di Mauro G, Lungu-Mitea S, Negrini P, Guarino AM, Frigato E, et al. Modulation of DNA Repair Systems in Blind Cavefish during Evolution in Constant Darkness. Current Biology. 2018;28: 3229–3243. doi:10.1016/j.cub.2018.08.039
56. Fumey J, Hinaux H, Noirot C, Thermes C, Rétaux S, Casane D. Evidence for late Pleistocene origin of Astyanax mexicanus cavefish. BMC Evol Biol. 2018;18: 43. doi:10.1186/s12862-018-1156-7
57. Herman A, Brandvain Y, Weagley J, Jeffery WR, Keene AC, Kono TJY, et al. The role of gene flow in rapid and repeated evolution of cave-related traits in Mexican tetra, Astyanax mexicanus. Mol Ecol. 2018;22: 4397–4416. doi:10.1111/mec.14877
58. Medley JK, Persons J, Biswas T, Olsen L, Peuß R, Krishnan J, et al. The metabolome of Mexican cavefish shows a convergent signature highlighting sugar, antioxidant, and Ageing-Related metabolites. Elife. 2022;11. doi:10.7554/eLife.74539
59. Aspiras A, Rohner N, Marineau B, Borowsky R, Tabin J. Melanocortin 4 receptor mutations contribute to the adaptation of cavefish to nutrient-poor conditions. Proceedings of the National Academy of Sciences. 2015;112: 9688–73.
60. Kozol RA, Yuiska A, Han JH, Tolentino B, Lopatto A, Lewis P, et al. Novel Husbandry Practices Result in Rapid Rates of Growth and Sexual Maturation Without Impacting Adult Behavior in the Blind Mexican Cavefish. Zebrafish. 2023;20: 86–94. doi:10.1089/zeb.2023.0001
61. Elipot Y, Legendre L, Père S, Sohm F, Rétaux S. Astyanax transgenesis and husbandry: how cavefish enters the laboratory. Zebrafish. 2014;11: 291–9. doi:10.1089/zeb.2014.1005
62. Domankevich V, Eddini H, Odeh A, Shams I. Resistance to DNA damage and enhanced DNA repair capacity in the hypoxia-tolerant blind mole rat Spalax carmeli. J Exp Biol. 2018;221. doi:10.1242/jeb.174540
63. Kozol R, Conith A, Yuiska A, Cree-Newman A, Tolentio B, Banesh K, et al. A brain-wide analysis maps structural evolution to distinct anatomical modules.

64. Jaggard JB, Lloyd E, Yuiska A, Patch A, Fily Y, Kowalko JE, et al. Cavefish brain atlases reveal functional and anatomical convergence across independently evolved populations. Sci Adv. 2020;6. doi:10.1126/sciadv.aba3126
65. Kumar R, R. Gullapalli R. High Throughput Screening Assessment of Reactive Oxygen Species (ROS) Generation using Dihydroethidium (DHE) Fluorescence Dye. Journal of Visualized Experiments. 2024. doi:10.3791/66238
66. Riddle MR, Boesmans W, Caballero O, Kazwiny Y, Tabin CJ. Morphogenesis and motility of the Astyanax mexicanus gastrointestinal tract. Dev Biol. 2018;441: 285–296. doi:10.1016/j.ydbio.2018.06.004
67. Jaggard JB, Lloyd E, Lopatto A, Duboue ER, Keene AC. Automated Measurements of Sleep and Locomotor Activity in Mexican Cavefish. J Vis Exp. 2019. doi:10.3791/59198
68. Dobin A, Davis CA, Schlesinger F, Drenkow J, Zaleski C, Jha S, et al. STAR: ultrafast universal RNA-seq aligner. Bioinformatics. 2013;29: 15–21. doi:10.1093/bioinformatics/bts635
69. Love MI, Huber W, Anders S. Moderated estimation of fold change and dispersion for RNA-seq data with DESeq2. Genome Biol. 2014;15: 550. doi:10.1186/s13059-014-0550-8

## Figure Legends

**Figure 1. Cavefish harbor increased neuronal DNA damage and gut ROS. (A,B)** Representative images of cells stained with DAPI and γH2AX in the rhombencephalon of surface fish **(A)** and cavefish **(B)**. Scale bar = 5 μm. **(C)** Mean γH2AX fluorescence across three regions of surface fish and cavefish brains. (rhomb: rhombencephalon; mes: mesencephalon; tele: telencephalon) (Mixed-effects analysis: $F_{1,\ 68} = 32.08$, $p < 0.0001$). **(D)** Representative image of larval gut showing regions in false color (re: rectum). **(E,F)** Representative images of surface fish and cavefish guts stained with DHE marking ROS. Scale bar = 500 μm. **(G)** Mean DHE fluorescence across four regions of surface fish and cavefish guts (two-way repeated measures ANOVA: $F_{1,\ 35} = 48.36$, $p < 0.0001$).

**Figure 2. Cavefish lack a sleep response to UV-B-induced DNA damage. (A)** The 24-hour sleep profiles of surface fish exposed to 30 or 60 seconds of UV-B light compared to controls. **(B)** Average sleep amount in surface fish in the 3 hours following UV-B exposure (one-way ANOVA: $F_{2,\ 202} = 18.75$, $p < 0.0001$). **(C)** Average bout length in surface fish in the 3 hours following UV-B exposure (one-way ANOVA: $F_{2,\ 201} = 8.301$, $p = 0.0003$). **(D)** Bout number in the 3 hours following UV-B exposure (one-way ANOVA: $F_{2,\ 201} = 11.5$, $p < 0.0001$). **(E)** The 24-hour sleep profiles of cavefish exposed to 30 or 60 seconds of UV-B light compared to controls. **(F)** Average sleep amount in cavefish in the 3 hours following UV-B exposure. **(G)** Average bout length in cavefish in the 3 hours following UV-B exposure. **(H)** Bout number in cavefish in the 3 hours following UV-B exposure. (ZT=Zeitgeber time). All treatments performed at ZT0.

**Figure 3. Transcriptional responses to UV-B-induced DNA damage in surface fish and cavefish. (A)** Schematic of experimental design. **(B)** Multidimensional scaling plot depicting the variances in principal component space between the processed sequencing samples. PC1 (two-way ANOVA: (Treatment) $F_{1,10}$=6.388, $p$=0.03, (Population) $F_{1,10}$=4970, $p$<0.0001, (Interaction) $F_{1,10}$=17.56, $p$=0.0019. PC2 (two-way ANOVA: (Treatment) $F_{1,10}$=465.0, $p$<0.0001, (Population) $F_{1,10}$=0.4969, $p$=0.497, (Interaction) $F_{1,10}$=18.56, $p$=0.0015 **(C)** Bi-directional volcano plot of changes in gene expression in surface and cave larvae after exposure to DNA damaging UV-B radiation. **(D)** Heat map of gene expression in DNA repair genes which responded significantly in UV-B-exposed surface fish.

**Figure 4.** Pachón cavefish-derived cells exhibit a lower UV-induced DNA damage response and repair compared to surface fish. **(A,B)** Immunostaining of CPD shows a similar DNA damage level induced by UV in surface fish and Pachón cavefish embryonic fibroblasts. White circles indicate the nuclear area by DAPI staining. Orange indicates CPD. Scale bar, 40 μm. *P*-values were determined by two-way ANOVA: $F = 0.09703$, $p = 0.7586$. ns $p = 0.6404$, **** $p < 0.0001$. **(C,D)** Western blot of γH2AX indicates a diminished DNA damage response in Pachón cavefish embryonic fibroblasts compared to surface fish cells. **(E,F)** Flow cytometry images and quantification for host cell reactivation assays in surface fish and Pachón cavefish embryonic fibroblasts. Red line sets the GFP positive signal threshold. *P*-values were determined by unpaired *t*-test. **(G)** Representative GFP images for host cell reactivation assays in surface fish and Pachón cavefish embryonic fibroblasts. Scale bars, 500 μm.

**Figure 5. Transcriptional response to aging is diminished in cavefish across tissues. (A)** Multidimensional scaling plot plotting the distances in principal component space between the brain samples. PC1 (two-way ANOVA: (Treatment) $F_{1,11}$=4.209, $p$=0.0648, (Population)

$F_{1,11}$=2133, $p$<0.0001, (Interaction) $F_{1,11}$=0.029, $p$=0.867 PC2 (two-way ANOVA: (Treatment) $F_{1,11}$=16.83, $p$=0.0018, (Population) $F_{1,11}$=0.0002, $p$<0.99, (Interaction) $F_{1,11}$=19.37, $p$=0.0011 **(B)** Number of differentially expressed genes in the aged condition across tissues. **(C)** Bi-directional volcano plot depicting differences in gene expression between young and aged brains. **(D)** Dot plot visualizing the top 8 activated and suppressed gene ontology terms in aged cavefish brains resulting from GSE analysis.

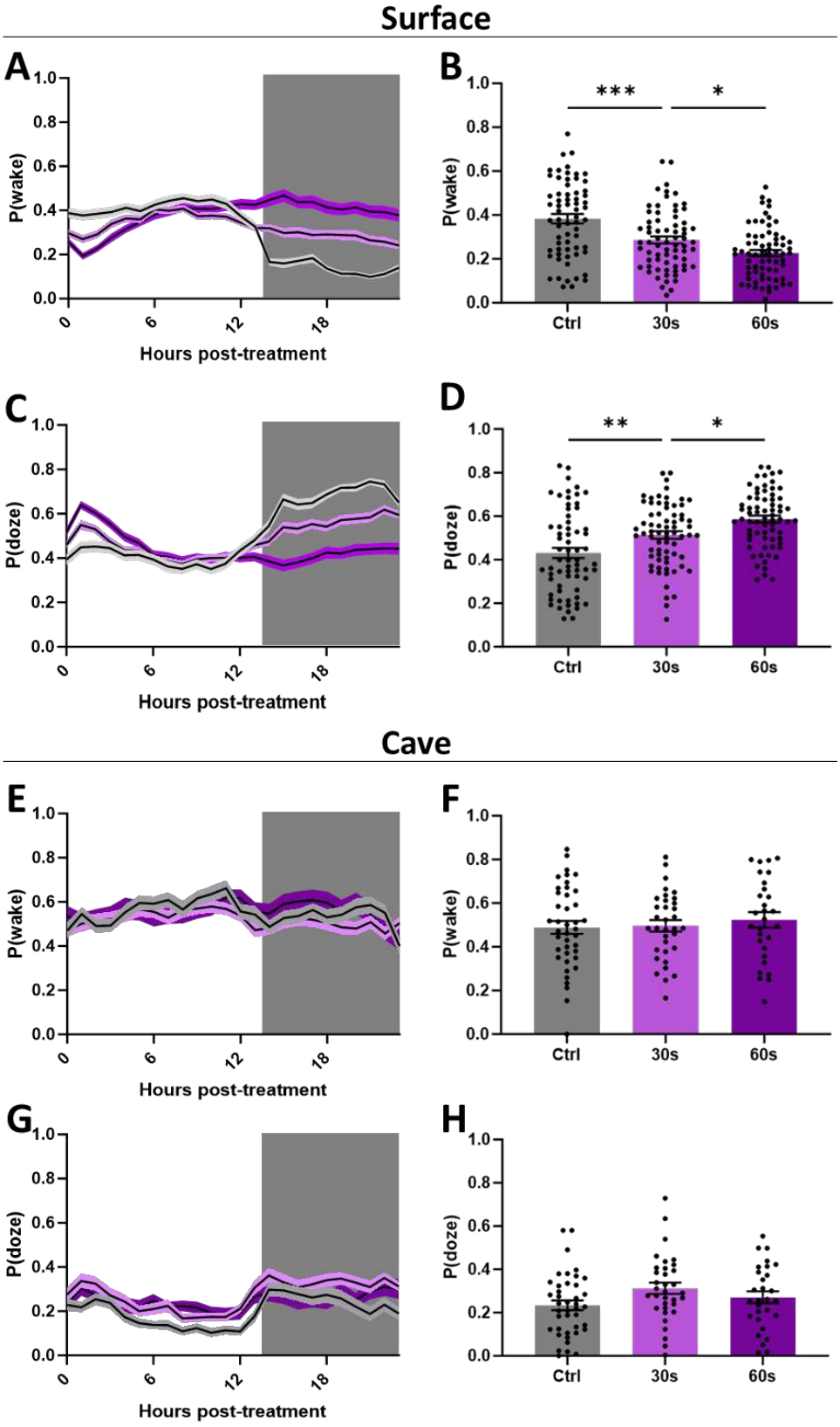

**Supplemental Figure 1. Response in sleep pressure to UV-B-induced DNA damage. (A)** The 24-hour P(wake) profiles of surface fish exposed to 30 or 60 seconds of UV-B light compared to controls. **(B)** P(wake) in surface fish in the 3 hours following UV-B exposure (one-way ANOVA: $F_{2, 202} = 21.08$, $p < 0.0001$). **(C)** The 24-hour P(doze) profiles of surface fish exposed to 30 or 60 seconds of UV-B light compared to controls. **(D)** P(doze) in surface fish in the 3 hours following UV-B exposure (one-way ANOVA: $F_{2, 202} = 14.09$, $p < 0.0001$). **(E)** The 24-hour P(wake) profiles of cavefish exposed to 30 or 60 seconds of UV-B light compared to controls. **(F)** P(wake) in cavefish in the 3 hours following UV-B exposure. **(G)** The 24-hour P(doze) profiles of cavefish exposed to 30 or 60 seconds of UV-B light compared to controls. **(H)** P(doze) in cavefish in the 3 hours following UV-B exposure. (ZT=Zeitgeber time). All treatments performed at ZT0.

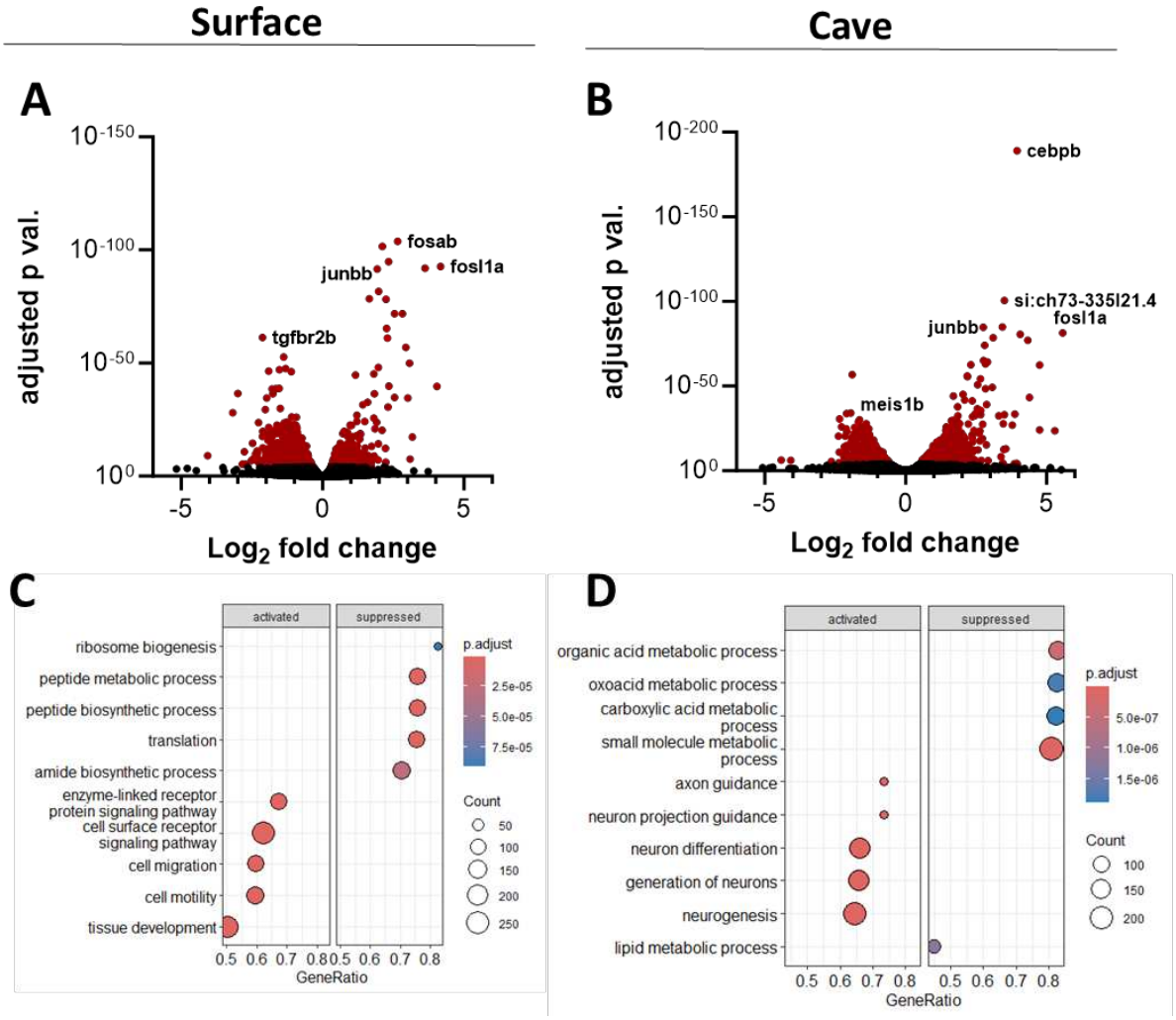


**Supplemental Figure 2. Transcriptional responses to UV-B-induced DNA damage in surface fish and cavefish. (A)** Volcano plot of gene expression in surface fish in response to UV-B radiation, with significant genes highlighted in red (adjusted $p < 0.05$). **(B)** Volcano plot of gene expression in cavefish in response to UV-B radiation, with significant genes highlighted in red (adjusted $p < 0.05$). **(C)** Most highly enriched GO terms in a gene set enrichment analysis of surface fish exposed to UV-B radiation. **(D)** Most highly enriched GO terms in a gene set enrichment analysis of cavefish exposed to UV-B radiation.

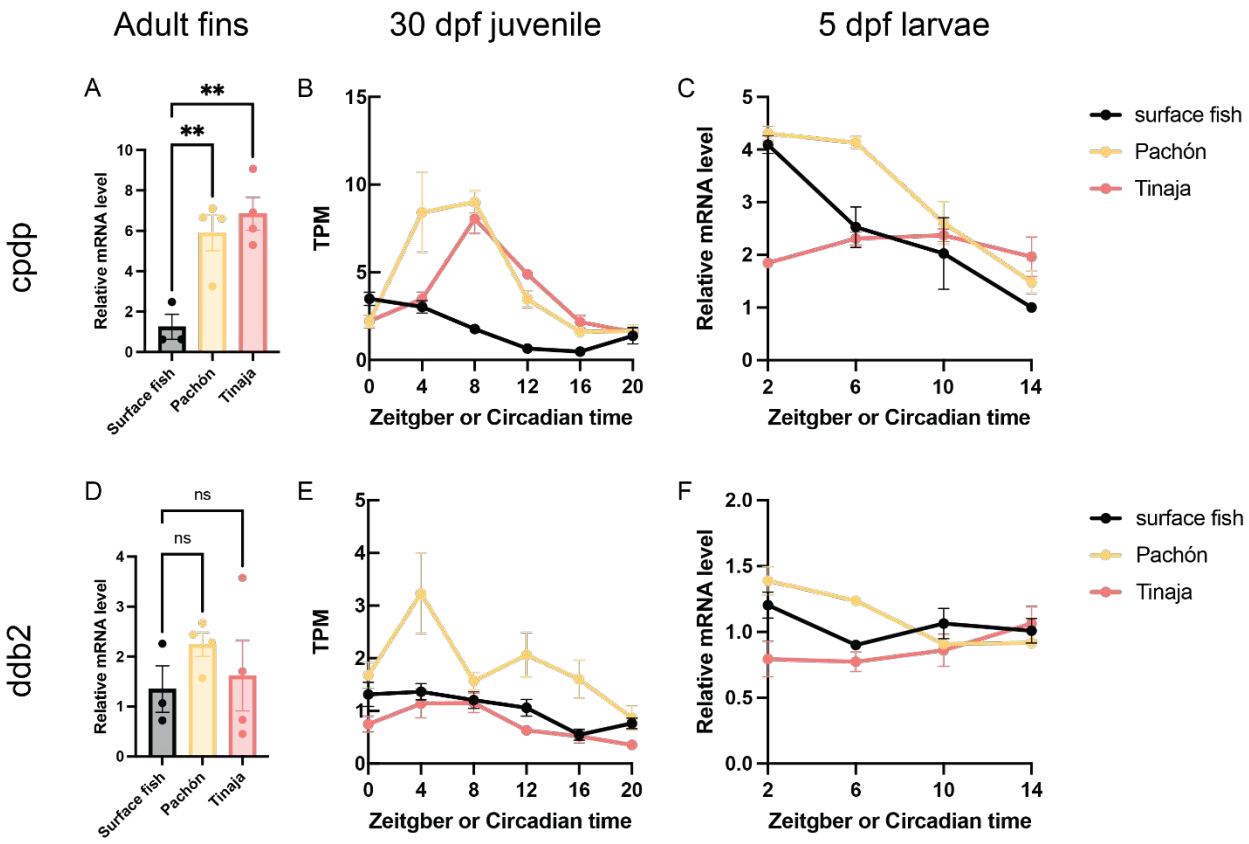


**Supplemental Figure 3. DNA repair gene expression in surface fish and cavefish. (A,D)** Adult fins were collected at Zeitgber or Circadian time 8. *cpdp* **(A)** and *ddb2* **(D)** mRNA levels were determined by qPCR. Expression of *cpdp* (one-way ANOVA: $F = 11.99$, $p = 0.0039$) and *ddb2* (one-way ANOVA: $F = 0.7576$, $p = 0.4997$) was compared among all populations. ns $p \geq 0.05$, ** $p < 0.01$. **(B,E)** RNA sequencing data obtained from *cpdp* **(B)** and *ddb2* **(E)** gene expression level in 30 dpf juvenile fish. (TPM: transcript per million). **(C,F)** Fish larvae aged 5 dpf were collected at different Zeitgber or Circadian times. *cpdp* **(C)** and *ddb2* **(F)** mRNA levels were determined by qPCR.

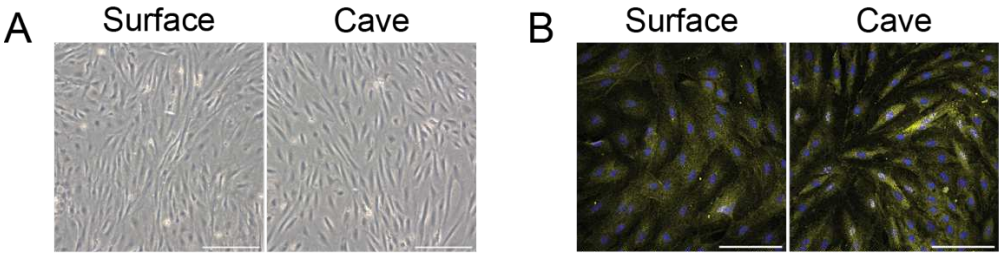


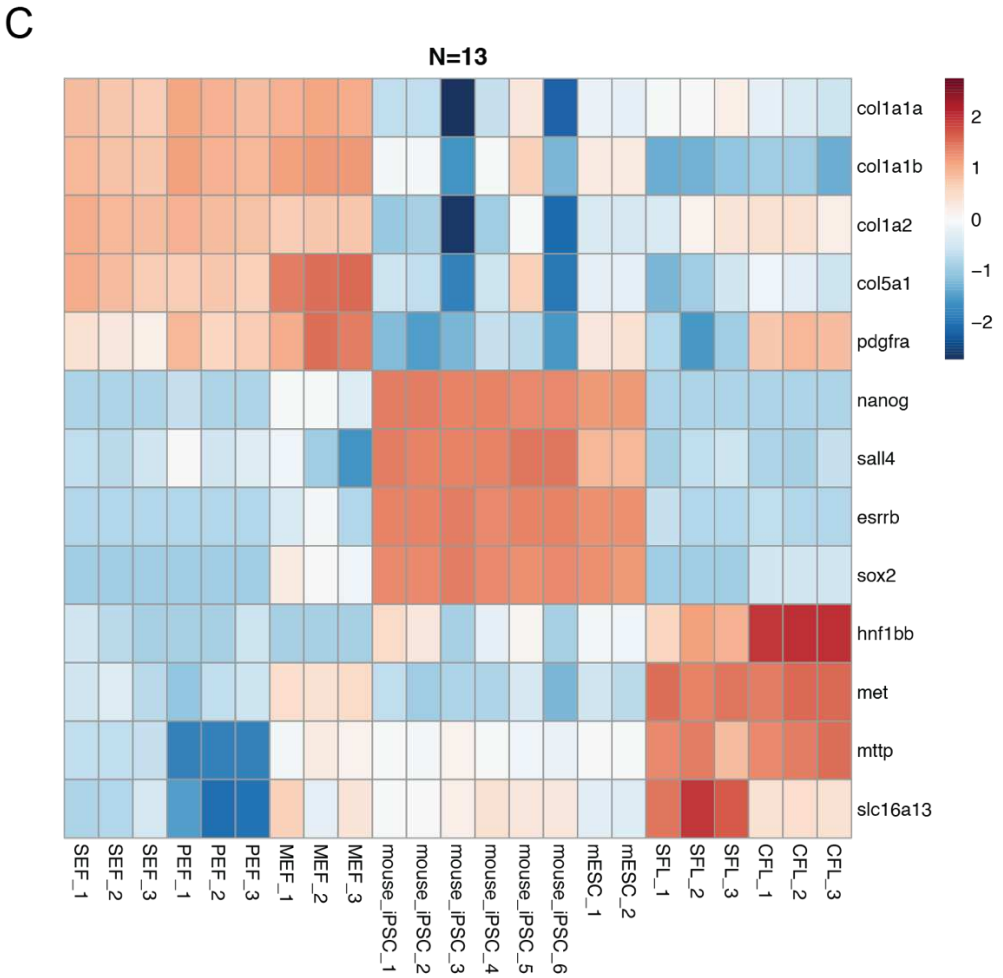


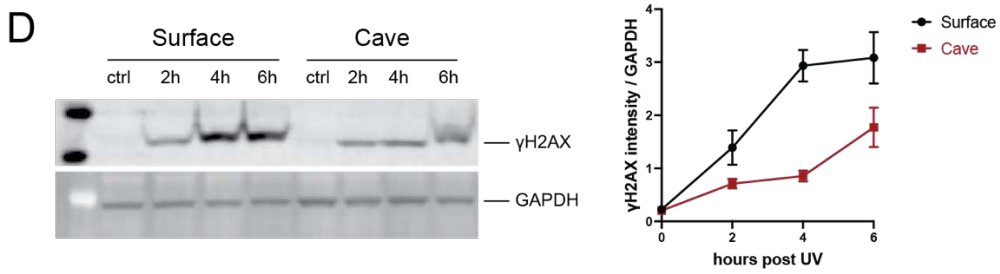

**Supplemental Figure 4. Pachón cavefish-derived cells exhibit a lower UV-induced DNA damage response and repair compared to surface fish. (A)** Bright field images of surface fish and Pachón cavefish embryonic fibroblasts. Scale bar, 200 μm. **(B)** Immunostaining of vimentin in surface fish and Pachón cavefish embryonic fibroblasts. Yellow and blue show vimentin and DAPI staining, respectively. Scale bar, 100 μm. **(C)** Heat map of differentially expressed genes among different cell types. The number below the heat map indicates independent biological replicates (n = 13). Red and blue indicate upregulated and downregulated genes, respectively. (SEF: surface fish embryonic fibroblast; PEF: Pachón cavefish embryonic fibroblast; MEF: mouse embryonic fibroblast; iPSC: induced pluripotent stem cell; mESC: mouse embryonic fibroblast; SFL: surface fish liver-derived cell; CFL: Pachón cavefish liver-derived cell). **(D)** Western blot of γH2AX indicates a diminished DNA damage response in Pachón cavefish liver-derived cells compared to surface fish liver-derived cells.

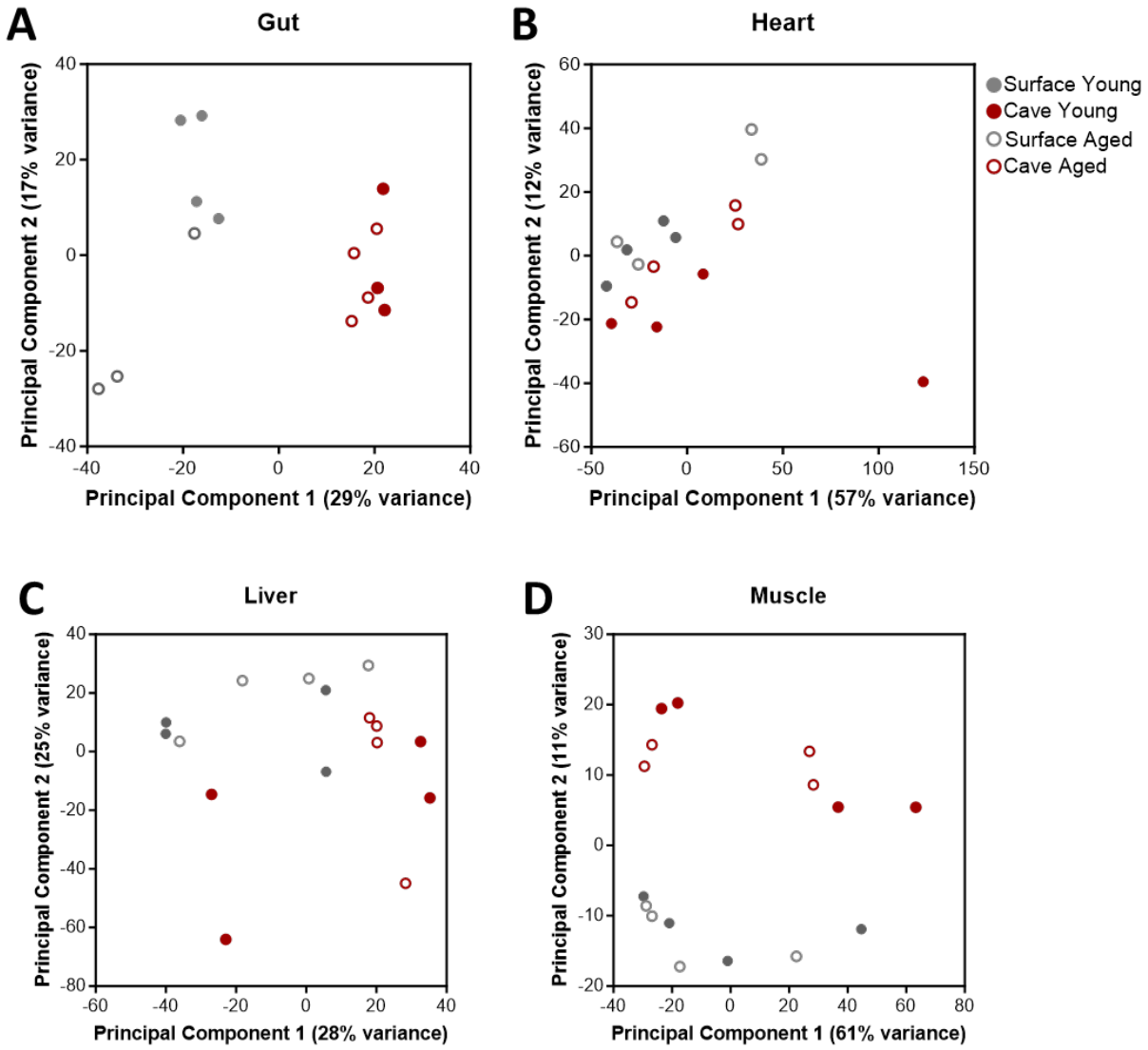


**Supplemental Figure 5. Aging-induced changes in gene expression.** Multi-dimensional scaling plots of gene expression in young and aged surface fish and cavefish samples, in the gut **(A)** PC1 (two-way ANOVA: (Treatment) $F_{1,11}$=10.41, $p$=0.0081, (Population) $F_{1,11}$=264, $p$<0.0001, (Interaction) $F_{1,11}$=3.135, $p$=0.1043. PC2 (two-way ANOVA: (Treatment) $F_{1,11}$=8.257, $p$=0.0151, (Population) $F_{1,11}$=0.594, $p$=0.4571, (Interaction) $F_{1,11}$=7.113, $p$=0.0219. Heart **(B)** PC1 (two-way ANOVA: (Treatment) $F_{1,12}$=0.0302, $p$=0.8649, (Population) $F_{1,12}$=0.8455, $p$=0.376, (Interaction) $F_{1,12}$=0.9535, $p$=0.3481. PC2 (two-way ANOVA: (Treatment) $F_{1,12}$=7.354, $p$=0.0189, (Population) $F_{1,12}$=0.7.584, $p$=0.0175, (Interaction) $F_{1,12}$=0.3345, $p$=0.5737. Liver **(C)** PC1 (two-way ANOVA: (Treatment) $F_{1,12}$=1.067, $p$=0.3219, (Population) $F_{1,12}$=4.521, $p$=0.0549, (Interaction) $F_{1,12}$=0.1329, $p$=0.7217. PC2 (two-way ANOVA: (Treatment) $F_{1,12}$=2.039, $p$=0.1788, (Population) $F_{1,12}$=6.986, $p$=0.0214, (Interaction) $F_{1,12}$=0.0419, $p$=0.8413. Muscle **(D)** PC1 (two-way ANOVA: (Treatment) $F_{1,12}$=0.5895, $p$=0.4574, (Population) $F_{1,12}$=0.7313, $p$=0.4092, (Interaction) $F_{1,12}$=0.01396, $p$=0.9079. PC2 (two-way ANOVA: (Treatment) $F_{1,12}$=0.15, $p$=0.7053, (Population) $F_{1,12}$=89.42, $p$<0.0001, (Interaction) $F_{1,12}$=0.009, $p$=0.9251.

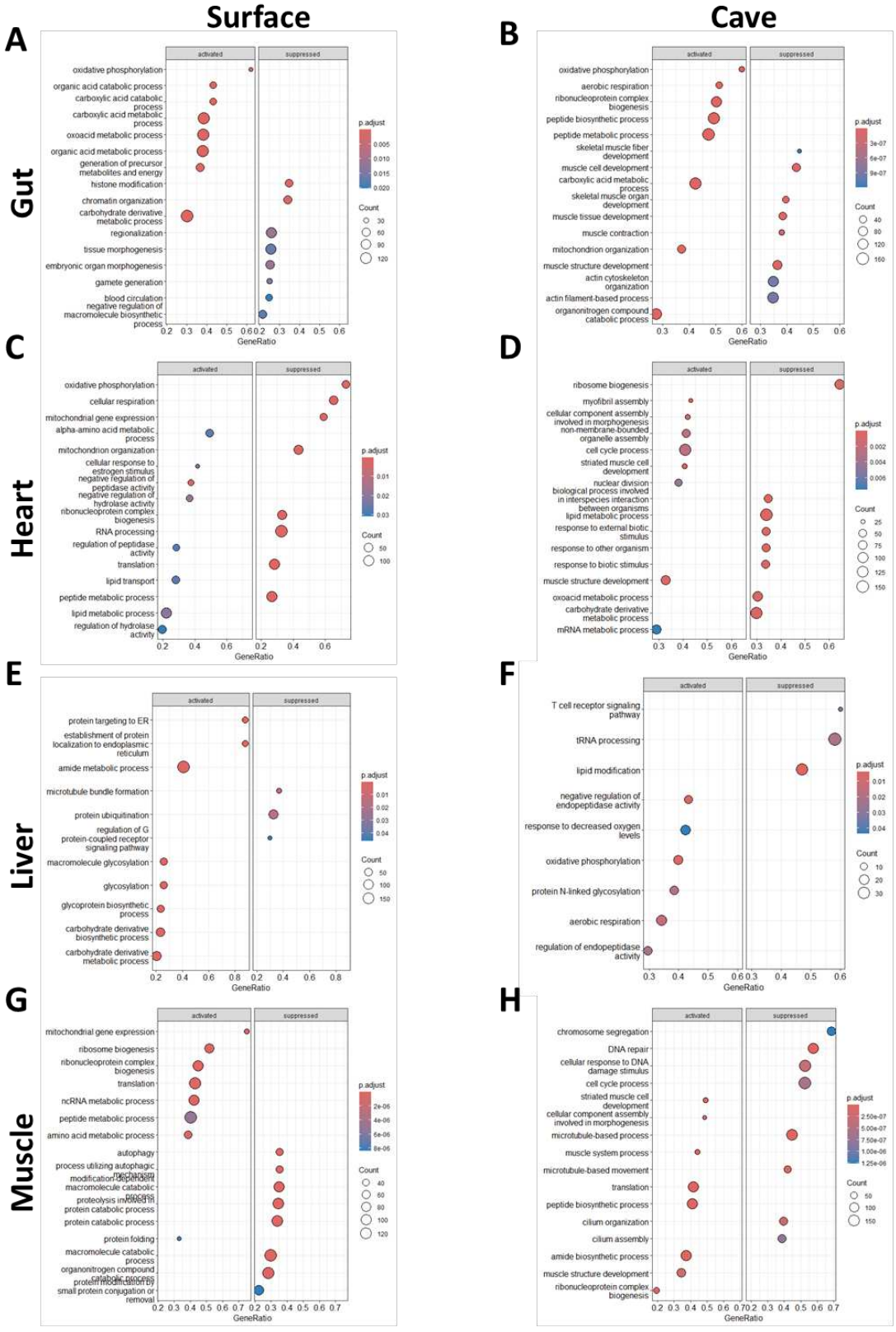


**Supplemental Figure 6. GSEA analyses of aging surface fish and cavefish tissues.** Top GO terms resulting from GSEA analysis in aged surface fish (left) and cavefish (right) tissues. Gut **(A,B)**, heart **(C,D)**, liver **(E,F)**, and muscle **(G,H).** Top 8 results in each direction are shown; if less than 8 terms were enriched, all results are shown.